Petroleum Science 21 (2024) 3675–3691

Contents lists available at ScienceDirect

Petroleum Science

journal homepage: www.keaipublishing.com/en/journals/petroleum-science

Original Paper

Microscopic occurrence and distribution of oil and water in situ shale: Evidence from nuclear magnetic resonance

Peng-Fei Zhang [a, b], Shuang-Fang Lu [b, *], Jun-Jie Wang [b], Wen-Biao Li [b, **], Ya-Jie Yin [a], Guo-Hui Chen [b], Neng-Wu Zhou [b], Han Wu [a]

[a] College of Earth Science and Engineering, Shandong University of Science and Technology, Qingdao, 266590, Shandong, China
[b] Sanya Offshore Oil & Gas Research Institute, Northeast Petroleum University, Sanya, 572025, Hainan, China

ARTICLE INFO

Article history:
Received 31 December 2023
Received in revised form
29 February 2024
Accepted 15 April 2024
Available online 18 April 2024

Edited by Jie Hao and Meng-Jiao Zhou

Keywords:
Pore water
Pore oil
Microscopic occurrence
Shale oil reservoir
Nuclear magnetic resonance
Gulong Sag

ABSTRACT

Characterizing the microscopic occurrence and distribution of in-situ pore water and oil is crucial for resource estimation and development method selection of shale oil. In this paper, a series of nuclear magnetic resonance (NMR) experiments were conducted on shales from the Gulong Sag, Songliao Basin, China, at AR, WR-AR, WOR-AR, Dry, SO, and WR states. In-situ pore water and oil were reconstructed after WOR-AR. An improved T_1–T_2 pattern for shale oil reservoirs comprising water and oil was proposed to classify and quantitatively detect pore fluids at different occurrence states. The total and free oil contents derived from NMR T_1–T_2 spectra at AR states were found to correlate well with those from multistage Rock-Eval. Moreover, the NMR-calculated total and free oil are generally larger than those measured from multistage Rock-Eval, whereas adsorbed oil is the opposite, which implies that adsorbed, bound, and movable oils in shale pores can be accurately and quantitatively detected via NMR, without absorbed hydrocarbons in kerogen. As per the NMR T_2 and T_1–T_2 spectra at WOR-AR state, the micro-distributions of in-situ pore water and oil were clearly demonstrated. Adsorbed, bound, and movable oils primarily occur in the micropores (<100 nm), mesopores (100–1000 nm), and macropores (>1000 nm), respectively, whereas capillary-bound water is primarily correlated with micropores. Thus, the microscopic occurrence and distribution of adsorbed oil are remarkably affected by pore water, followed by bound oil, and movable oil is hardly affected. This study would be helpful in further understanding the microscopic occurrence characteristics of pore fluids in-situ shale oil reservoirs.

1. Introduction

Shale oil is described as mature oil existing in shale series, which comprise hydrocarbons and nitrogen, sulfur, and oxygen (NSO)-bearing complex compounds (Li et al., 2018a; Zhao et al., 2020). Shale oil primarily occurs in adsorbed and free states, and free oil can be further classified into bound and movable oil according to its liquidity (Li et al., 2016, 2017a; Wang et al., 2022a; Zhang et al., 2022a). Free oil, especially movable oil, is the primary development target resource (Hu et al., 2021; Xu et al., 2022). In addition, the microscopic occurrence and production of shale oil are commonly affected by pore water (Sang et al., 2022; Zhang et al., 2022b). Consequently, the analyses of microscopic occurrence and distribution of water and oil in pore networks are crucial for the resource estimation and development method selection of shale oil.

With adsorbed and free oil bearing no noticeable difference, it is difficult to determine the micro-occurrence of shale oil (Li et al., 2017a; Tian et al., 2018). Recently, chloroform asphalt "A" extracted from shale has been commonly used to evaluate shale oil contents, but it loses light hydrocarbons (Xue et al., 2016). Furthermore, Rock-Eval is currently the most common experiment used to characterize shale oil content (Lu et al., 2012). The volatile hydrocarbons (S_1) detected at 300 °C are generally regarded as free oil. However, it does not include light and heavy hydrocarbons (Xue et al., 2016; Zhang et al., 2022c). Both chloroform asphalt "A" and S_1 cannot indicate the shale oil in adsorbed and free states. As a result, a multistage Rock-Eval technique was used to analyze shale oil in different states (Jiang et al., 2016; Hu et al., 2021; Li et al., 2022). During the multistage Rock-Eval experiments, $S_{1\text{-}1}$, i.e., light oil, can be first detected at the temperature of 200 °C; thereafter, the

* Corresponding author.
** Corresponding author.
E-mail addresses: lushuangfang@nepu.edu.cn (S.-F. Lu), liwenbiao@nepu.edu.cn (W.-B. Li).

https://doi.org/10.1016/j.petsci.2024.04.007

temperature increases to 300 °C to obtain $S_{1\text{-}2}$ (light–medium). Moreover, $S_{1\text{-}1}$ and $S_{1\text{-}2}$ have been regarded as free oil (Zhang et al., 2022c). When the temperature continues to increase from 300 °C to 450 °C, the adsorbed oil ($S_{2\text{-}1}$) is detected (Jiang et al., 2016), and kerogen-derived hydrocarbons ($S_{2\text{-}2}$) are finally determined between 450 °C and 600 °C. As discussed, chloroform asphalt "A" and Rock-Eval techniques only focus on the oil in shale.

Furthermore, the microdistributions of residual oil in shales can be determined by LTNA/D and MICP on samples before and after extraction, indicating that residual oil primarily occurs in micropores (<100 nm) (Wang et al., 2019; Bai et al., 2022; Lin et al., 2024). However, the difference in pore size distributions before and after extraction may also be attributed to the loss of pore water. Meanwhile, the influence of pore water has been ignored. Few studies have investigated the microdistribution of pore water in shale oil reservoirs. Investigations on pore water are primarily focused on high-over-maturity shale gas reservoirs (Zolfaghari et al., 2017; Feng et al., 2018; Cheng et al., 2018; Chen et al., 2021a; Fan et al., 2023; Li et al., 2024). Nevertheless, the microscopic occurrence and distribution of shale oil are obviously controlled by pore water. Shale samples should be powdered for extraction, Rock-Eval, and LTNA/D experiments, resulting in not only the pore structure being damaged but also both pore water and oil loss.

As a non-destructive and efficient technique, low-field NMR has been commonly used to characterize shale oil reservoirs. The traditional 1D T_2 spectrum has been successfully applied to examine the porosity, permeability, pore size distribution, etc. (Li et al., 2015; Zhang et al., 2018, 2022d, 2023a; Zhao et al., 2020; Liu et al., 2020, 2021; Wang et al., 2022b). However, the T_2 spectrum provides limited information and cannot accurately distinguish various proton populations in shale oil reservoirs. Moreover, the 2D NMR can provide additional resolutions in characterizing shales, especially the T_1–T_2 technique (Fleury et al., 2013; D'Agostino et al., 2014). Previous studies indicated that various proton populations have been successfully identified in the T_1–T_2 spectrum (Birdwell and Washburn, 2015; Habina et al., 2017; Jia et al., 2018; Liu et al., 2019, 2022; Li et al., 2020; Zhang et al., 2023b). According to T_2 and T_1/T_2 values, the T_1–T_2 spectrum can be divided into different regions, which are related to kerogen, structural water, adsorbed oil, and free oil. Moreover, a series of T_1–T_2 patterns have been proposed for shales (Fleury and Romero-Sarmiento, 2016; Li et al., 2018b; Zhang et al., 2020). T_1/T_2 values are associated with the fluidity of shale pore fluids, wherein a larger T_1/T_2 value primarily corresponds to weaker liquidity (Fleury and Romero-Sarmiento, 2016; Li et al., 2020). The signal amplitudes of inorganic and organic hydrogen-bearing components can be quantitatively obtained from the T_1–T_2 spectrum. The amplitudes of organic hydrogen-bearing components are noted to be consistent with Rock-Eval parameters, such as S_1, TOC, etc. (Li et al., 2018b; 2020). However, previous studies primarily focused on the T_1–T_2 spectra of AR or SO shales (Li et al., 2018b; 2020; Liu et al., 2019; Zhang et al., 2020). During coring, preservation, and pretreatment processes, both water and oil may escape from the shale pore networks, leading to changes in the micro-occurrence of pore oil and water. Moreover, the SO state overlooks the water in shale pore networks. Significant challenges remain in characterizing the occurrence of in-situ pore fluids in shale.

Thus, this study aims to clarify the microscopic occurrence and distribution of in-situ pore oil and water in shale oil reservoirs. To achieve this goal, a series of NMR tests were conducted on the shale samples from the Gulong Sag, Songliao Basin, China, at AR, WR-AR, WOR-AR, Dry, SO, and WR states. Meanwhile, an innovative water and oil restoration method for AR shales were proposed. Such analyses allowed for the generation of an improved T_1–T_2 pattern, which served as a framework for identifying and quantitatively detecting the in-situ pore fluids at different occurrence states. The evaluation results of shale oil from NMR were compared with multistage Rock-Eval parameters. Moreover, the effect of pore water on shale oil was also discussed and the microdistributions of pore water and oil in in-situ shale oil reservoirs were clarified.

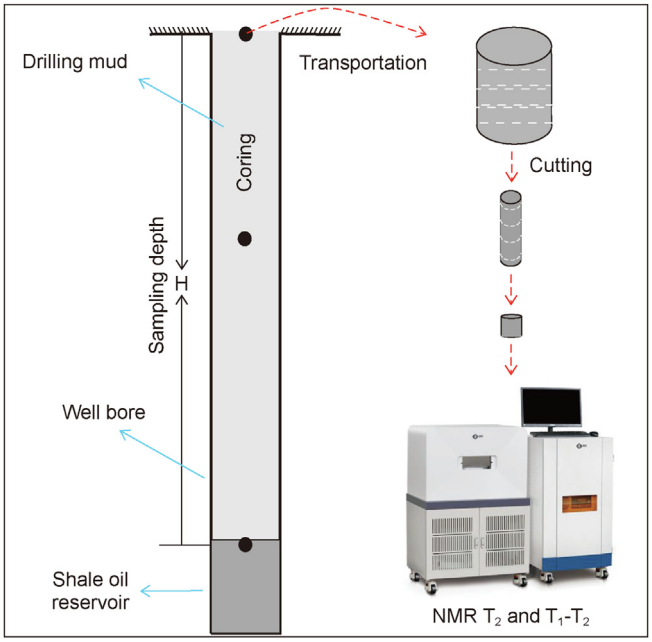

Fig. 1. Work flows of sampling.

2. Methodology

2.1. Samples

In this study, the analyzed shales were sampled from the Cretaceous Qingshankou Formation in the Gulong Sag, Songliao Basin, China. Gulong Sag is located in the Central Depression of Songliao Basin and is known to contain thick, organic-rich shales with excellent potential for shale oil (Jin et al., 2022). The first and second members of the Qingshankou Formation are the primary source rocks with a high TOC content of 1.0%–4.0% and types I/II kerogen, corresponding to the high content of S_1, ranging from 2 mg/g to 10 mg/g (Huangfu, et al., 2023). The organic matter is characterized by high maturity, and R_o is generally greater than 1%, resulting in the medium to high-maturity shale oil developing in the Gulong Sag (He et al., 2023).

In total, twelve shale samples were selected from the shale oil boreholes in the Gulong Sag. The shales were carefully packed with preservative film and quickly transported to the laboratory for cutting. All samples were cut parallel to the bedding surface into core plugs (approximately 25 mm in diameter and 30 mm in length) using wire-cutting techniques under waterless conditions. The core plugs were used for NMR experiments, while core cuttings were crushed into powder (>100 mesh) to conduct TOC, Rock-Eval, and X-ray diffraction tests.

2.2. NMR experimental process

Before the NMR tests, the shale samples underwent coring, packaging, transportation, cutting, etc., as shown in Fig. 1. During these processes, due to changes in the environment (temperature, pressure, RH, etc.), the shale pore water and oil would escape,

resulting in water and oil losses (Li et al., 2020; Zhang et al., 2022c). To restore the water and oil in shale, and calibrate the amplitude in the T_1–T_2 spectrum, two series of NMR experiments were planned, as illustrated in Fig. 2. The first NMR experimental process aims to restore the water and oil and calibrate the amplitude of oil, in five steps: AR, WR-AR, WOR-AR, Dry, and SO, marked as the serial numbers 1-1 to 1–4, as displayed in Fig. 2.

The AR shales are the cut samples with no treatment. Subsequently, the AR shales were placed in a controlled RH chamber to restore water, i.e., water vapor adsorption (equilibrium moisture), which is regarded as the reverse process of pore water volatilization in the open air. Shale pore water is liquid under geological conditions (Li et al., 2019, 2024). If the RH of the open air is low, the pore water will continue to evaporate. A high RH is necessary to restore pore water. Hence, the saturated salt solution of K_2SO_4 was used to control high RH of approximately 98% (Li et al., 2017b; Feng et al., 2018). The water sorption process continued until the shale quality remained constant, which is called WR-AR. The WR-AR shales were then saturated with light oil (n-dodecane) to restore pore oil, a process known as WOR-AR. As a result, a novel approach for restoring pore oil and water of the AR shale, water adsorption followed by saturated light oil, has been developed. The WOR-AR state can be used to efficiently define the in-situ pore fluids in shale oil reservoirs. The WOR-AR shales were washed oil by the mixed solution of dichloromethane and acetone (3:1 in volume) at 80 °C for 7 days and then dried at 110 °C for 24 h under vacuum condition to remove all the water and oil in shale pores. Finally, the dry shales were saturated with n-dodecane to obtain the SO state.

The second NMR experimental process aims to calibrate the amplitude of water in the T_1–T_2 spectrum, marked as the serial numbers 2–1 to 2-2 in Fig. 2. After the AR shales were washed oil and dried using the same method, water sorption was conducted in a controlled RH chamber, called WR. In this study, the standard NMR tests were performed on the shale samples at AR, WR-AR, WOR-AR, Dry, SO, and WR states. Six T_2 and T_1–T_2 spectra were collected for each sample.

For NMR experiments, an NMR spectrometer MesoMR12-060H–I (Niumag, Suzhou, China) was used to collect T_2 and T_1-T_2 spectra. The CPMG and SR-CPMG sequences were employed to detect T_2 and T_1-T_2 spectra, respectively. The CPMG sequence parameters were set as follows: TW = 3000 ms, TE = 0.07 ms, NECH = 4096, and NS = 32. SR-CPMG sequences parameters were consistent with CMPG, except for TW = 10 ms and NTI = 31. All the fluids in shale pores, together with any partial (pseudo-)solid protons, can be detected using the extremely low TE of 0.07 ms (Zhang et al., 2020).

3. Results and discussion

3.1. Characteristics of the examined shales

3.1.1. Organic geochemical and mineral composition characteristics

The analyzed shales have large TOC content, ranging from 1.36% to 3.27%, with a mean of 2.12% (Table 1). The average value of S_1 is 2.26 mg/g, ranging from 1.33 mg/g to 4.82 mg/g. These shales primarily consist of quartz, feldspar, and clay minerals (Table 1 and Fig. 3(a)). Clay minerals vary from 29.3% to 48.6% (mean 36.6%), characterized by the largest contents. The contents of quartz are between 31.8% and 37.8%, with an average of 35.4%, followed by feldspar with a mean of 22.4% (10.3%–30.4%). Moreover, there are small amounts of calcite (mean 1.6%), dolomite (mean 2.7%), and pyrite (mean 4.5%). According to three terminal elements of felsic

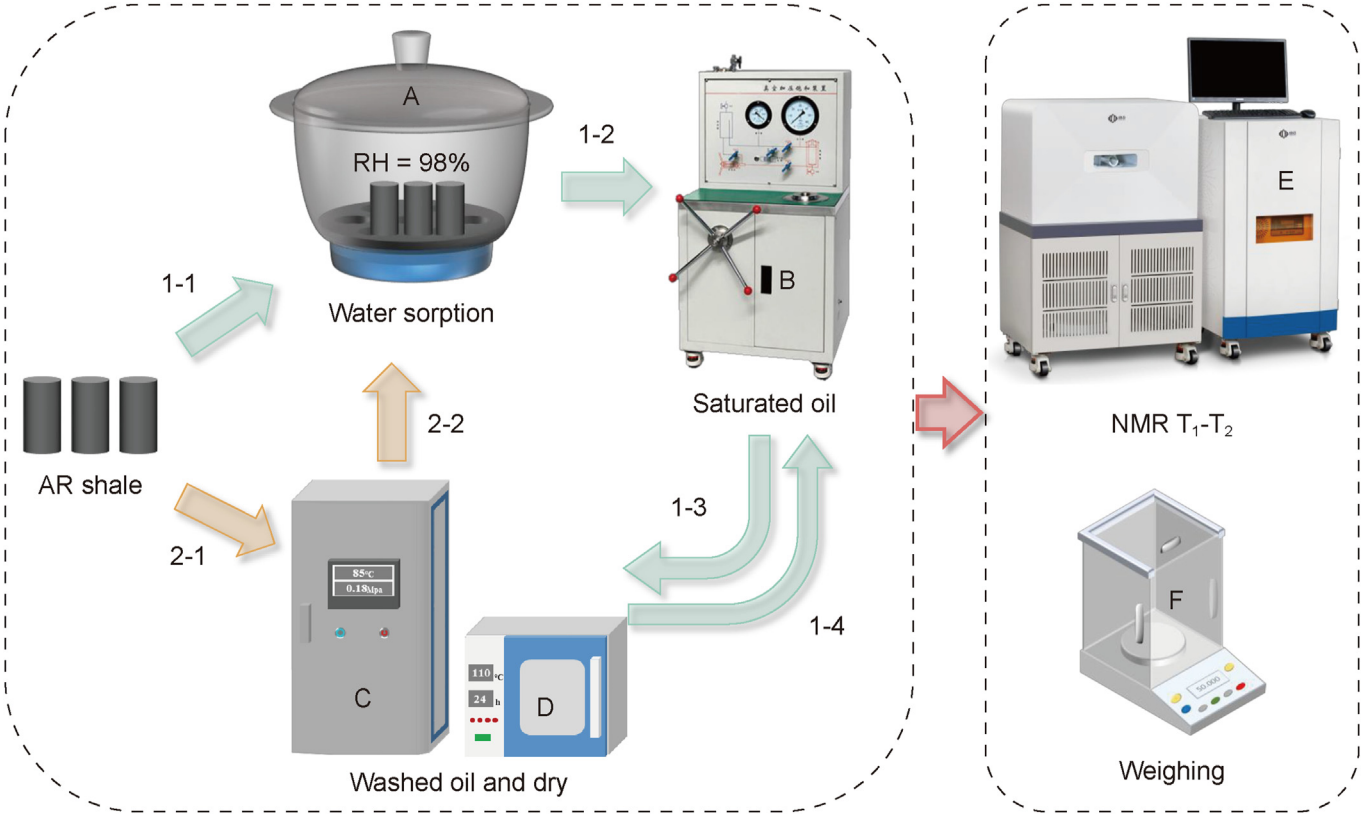

Fig. 2. NMR experimental process. A is the controlled RH chamber; B is the vacuum pressure saturator; C is the oil-cleaned instrument and D is the vacuum drying oven; E is the NMR spectrometer MesoMR12-060H–I; F is the electronic balance. The serial numbers 1-1 to 1–4 and 2–1 to 2-2 refer to these two NMR experimental processes, respectively.

Table 1
TOC, S_1, and mineral compositions of selected shales.

Sample	Depth, m	TOC, %	S_1, mg/g	Quartz, %	Feldspar, %	Calcite, %	Dolomite, %	Pyrite, %	Clay minerals, %
SY1	2332.76	2.06	1.91	37.8	22.7	/	/	5.0	34.6
SY2	2340.75	2.84	2.15	35.3	22.5	/	2.9	4.3	35.0
SY3	2344.80	2.09	2.67	35.6	29.5	1.1	/	4.1	29.6
SY4	2349.28	1.99	2.34	35.5	16.7	1.3	/	6.3	40.2
SY5	2353.98	1.78	1.74	35.2	30.4	1.5	/	3.5	29.3
SY6	2355.14	1.36	1.33	36.1	19.7	1.9	/	4.2	38.1
SY7	2358.38	1.70	1.95	36.7	28.8	/	/	3.9	30.6
SY8	2345.58	1.89	2.13	35.0	27.3	0.9	/	4.0	32.9
SY9	2390.67	2.53	2.53	31.8	20.4	/	/	6.4	41.3
SY10	2390.25	2.11	1.71	34.5	20.5	0.8	/	3.9	39.4
SY11	2432.26	1.77	1.86	34.3	19.5	0.5	2.5	4.2	39.0
SY12	2439.25	3.27	4.82	36.7	10.3	4.4	/	/	48.6

Note: The mark "/" indicates that it has not been detected.

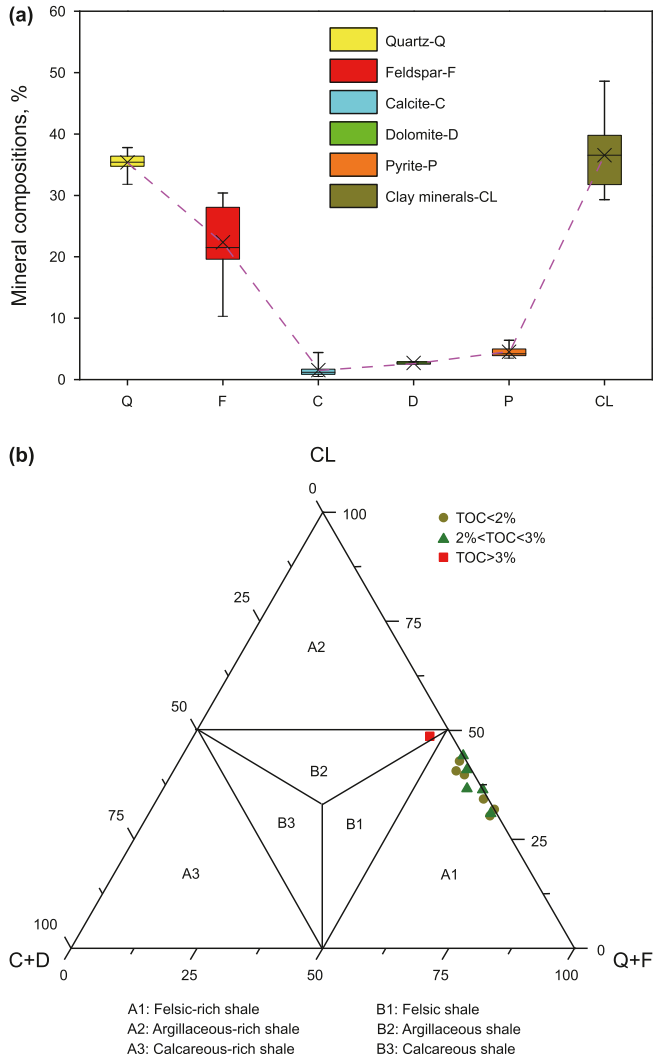

Fig. 3. Mineral compositions **(a)** and lithofacies **(b)** of analyzed shales.

(quartz and feldspar), calcareous (calcite and dolomite), and clay minerals, the selected shales are primarily classified as felsic-rich shales, except for one argillaceous shale sample (Fig. 2(b)), implying that the examined shales in Gulong Sag are mainly composed of brittle minerals.

3.1.2. Pore types

The high contents of brittle and clay minerals can often result in the development of interparticle pores at the edge of brittle granules (Fig. 4(a)–(d), (f), and (g)) and the intraparticle pores in clay mineral aggregates (Fig. 4(c), (d), and (j)). Moreover, interparticle pores between brittle granules, dissolution pores in quartz, and fractures are also identified, as displayed in Fig. 4(b), (d), (f), and (j). Intercrystalline pores are observed in pyrite aggregates (Fig. 4(b)). The development of pores associated with clay minerals may result in large contents of capillary-bound water and oil in shale pore systems.

3.2. NMR T_2 and T_1–T_2 spectra

3.2.1. NMR T_2 spectra

The T_2 spectra of the analyzed shales at different states are displayed in Fig. 5. Three distinct peaks can be identified. For the AR, WR-AR, and WOR-AR shales, the T_2 spectra are characterized by the dominant p1 but small p2 and p3 peaks. As compared with AR shales, the p1 peaks of WR-AR shales are noted to increase and move toward the larger T_2 values, while the p2 peaks move toward the larger T_2, but amplitude remains almost unchanged. This means that the p1 peak primarily relates to pore water. However, after water and oil restoration, the p1 peak is slightly lower than that of the WR-AR state. This is because pore water escapes during the oil-saturated process. On the contrary, p2 peaks increase and move toward the larger T_2, especially samples with larger p2 peaks, such as SY9 and SY12 (Fig. 5(e) and (f)). It indicates that the more developed the large pores, the higher the content of light components and the greater the loss of shale oil. Moreover, p3 peaks can also be observed in the WOR-AR shales. Thus, it can be concluded that p2 and p3 are mainly associated with shale pore oil.

The SO shales are all characterized by three distinct peaks, i.e., p1 < 1 ms, 1 ms < p2 < 20 ms, and p3 > 20 ms, which is consistent with the authors' previous studies, corresponding to micropores (<100 nm), mesopores (100–1000 nm), and macropores (>1000 nm) (Zhang et al., 2018, 2019). However, the WR shales have dominant p1 peaks, without p2 and p3 peaks, further indicating that the p1 peak primarily reflects shale pore water. Moreover, the T_2 spectra of dry shales have the least amplitudes, mainly related to the (pseudo-)solid protons in clay mineral-bound water, kerogen, etc. (Zhang et al., 2020). These results also imply that the 1D T_2 spectrum has failed to distinguish water and oil in shale pore systems effectively.

3.2.2. NMR T_1–T_2 patterns

Previous studies have focused on the NMR T_1–T_2 patterns for

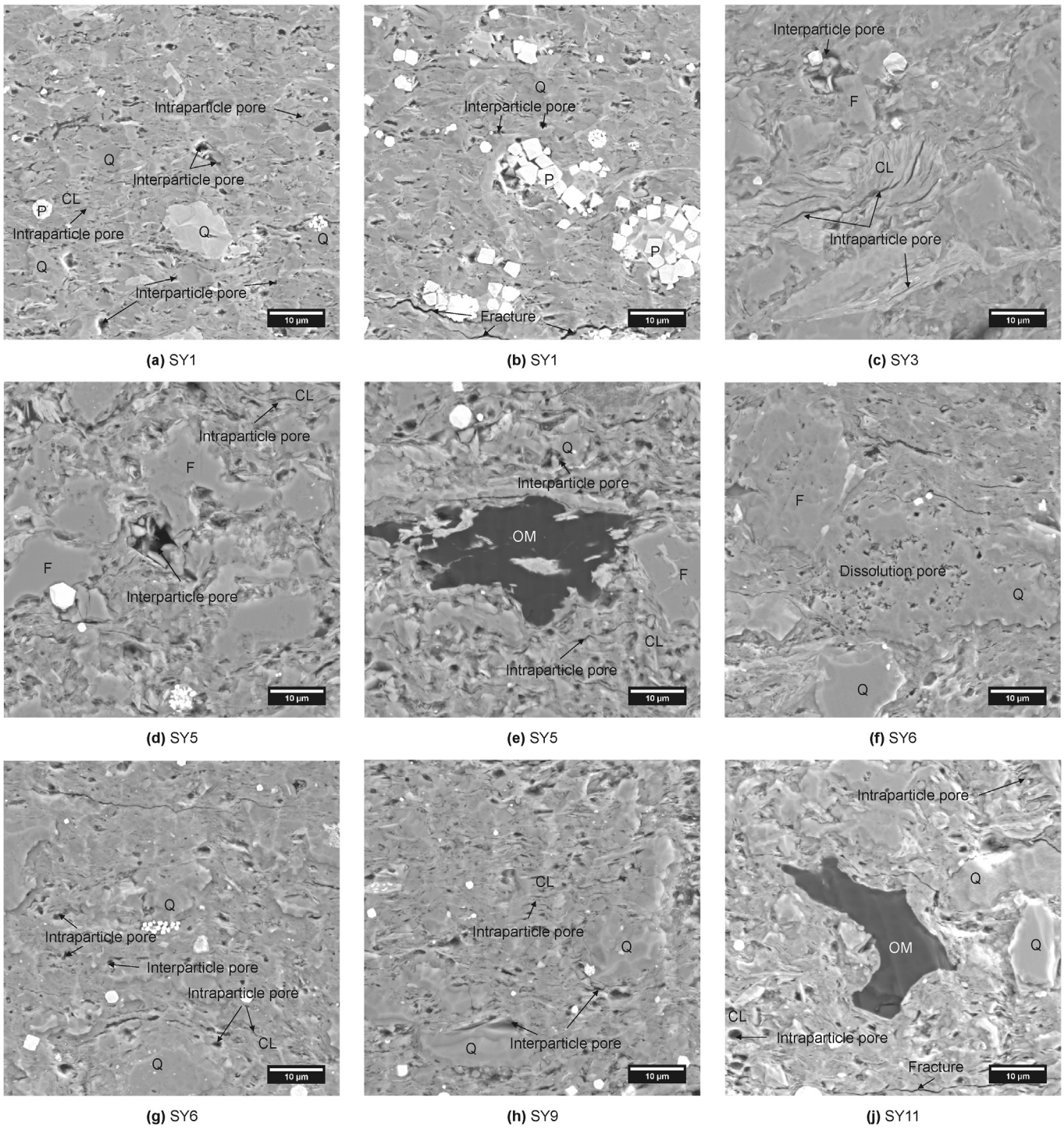

Fig. 4. Pore types in the studied shales. Q, CL, F, P, and OM represent the quartz, clay minerals, feldspar, pyrite, and organic matter, respectively.

shales; in fact, several patterns have already been determined (Fleury et al., 2013; Li et al., 2018b; Zhang et al., 2020). According to the T_1–T_2 pattern of Fleury and Romero-Sarmiento (2016), water, methane in porous media, kerogen, and hydroxyls could be identified. Based on this pattern, an improved T_1–T_2 pattern was proposed to distinguish hydrogen-bearing components in shale oil reservoirs, such as kerogen, adsorbed oil, free oil, structural and adsorbed water, and free water (Li et al., 2018b). In the authors' previous study, a T_1–T_2 pattern of oil-bearing shale fluids or protons was also drawn, in which eight hydrogen-bearing components were identified, such as crystal water, kerogen, nanopore oil, macropore oil, pore water, etc. (Zhang et al., 2020).

However, these T_1–T_2 patterns were hardly used to analyze the T_1–T_2 spectra of the collected shales due to the complex compositions of minerals and fluids. To determine the T_1-T_2 pattern, this study analyzed a large number of T_1-T_2 spectra of actual shale samples. Combined with clustering analysis method, the criteria for regional division were determined and eight regions were

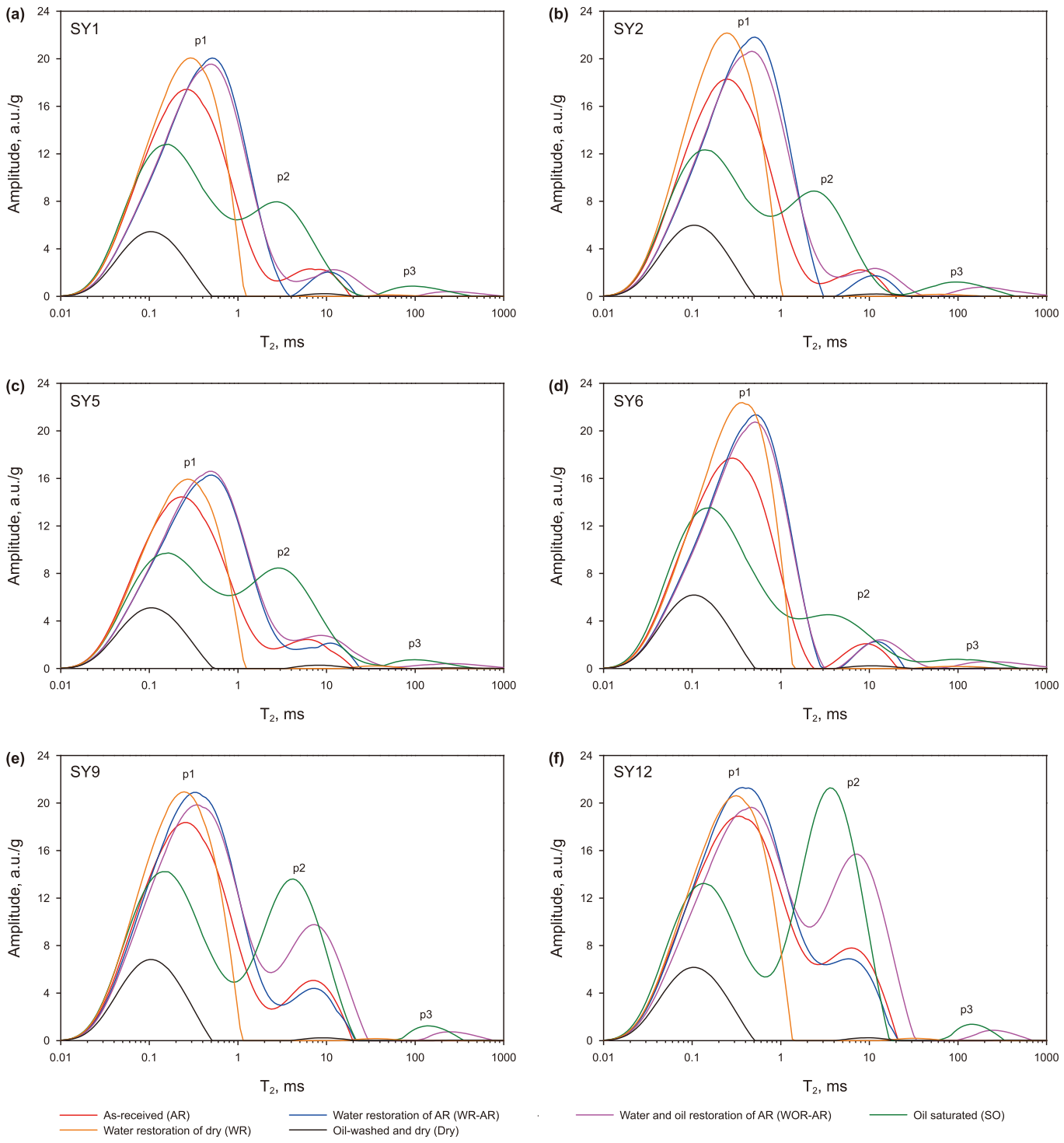

Fig. 5. T_2 spectra at different states of studied shales.

identified in T_1-T_2 spectra. Thus, based on previous T_1–T_2 patterns, an improved T_1–T_2 pattern for shale oil reservoirs containing oil and water was introduced, including eight components marked as regions A–H in Fig. 6(a).

The T_1–T_2 pattern can be primarily divided into two parts: pore fluids (A–E) and (pseudo-)solid protons (F–H), taking $T_2 = 0.1$ ms as a boundary. The most remarkable peak is the capillary-bound water, marked as A in the T_1–T_2 pattern. The capillary-bound water has a lower T_2 value of 0.1–1 ms and a lower T_1/T_2 value of less than 10. Above the capillary-bound water, a weak peak can be identified and marked as B, which refers to adsorbed oil in pores. Adsorbed oil has a similar T_2 value distribution of 0.1–1 ms but a T_1/T_2 value larger than 10. Region C denotes the bound oil with T_2 ranging from 1 ms to 20 ms and a T_1/T_2 value larger than 10. When the T_2 increases, the movable oil can be observed, which is then marked as D. Movable oil has the largest T_2 values of more than 20 ms. Moreover, the peak with T_2 larger than 1 ms and a lower T_1/T_2 value of approximately 2 refers to the movable water, marked E in

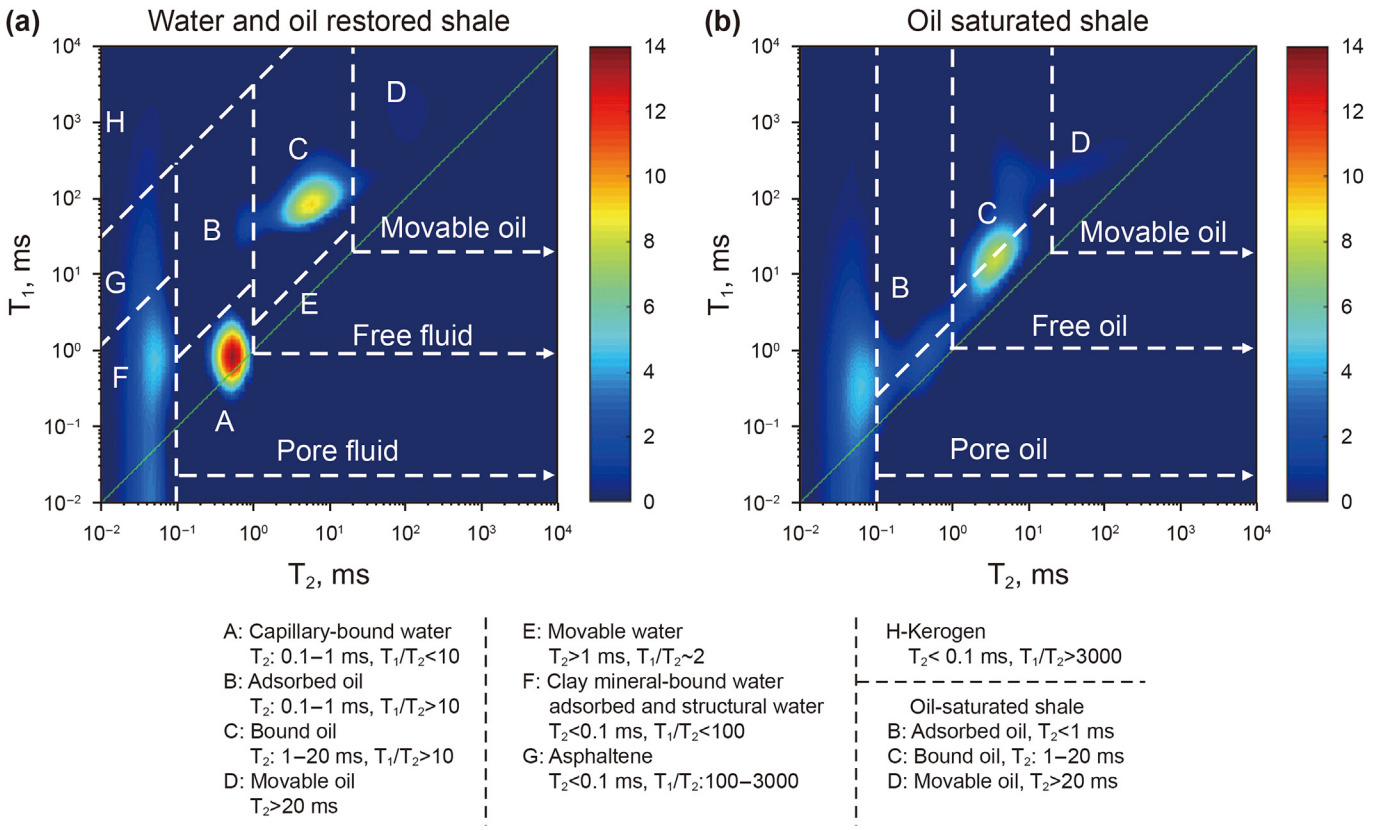

Fig. 6. T_1-T_2 patterns of shale after water and oil restoration **(a)** and oil-saturated **(b)** (SY12 as an example).

the T_1–T_2 pattern. Compared with shale pore water, pore oil has a larger T_1/T_2 value and is located above pore water in the T_1–T_2 spectrum.

Clay mineral-bound water (marked as F) has the lowest T_2 value of less than 0.1 ms and the T_1/T_2 value of less than 100. In this study, clay mineral-bound water uniformly refers to adsorbed and structural water, which is deemed almost immovable during shale oil development. Most of inorganic minerals are hydrophilic, especially clay minerals (Cheng et al., 2022). Strong hydrophilicity enables strong binding between adsorbed water and clay minerals, resulting in a lower T_2 value but a larger T_1/T_2 value of adsorbed water, mainly located in Region F. Correspondingly, the adsorbed water overlaps with the structural water in the T_1-T_2 spectrum. Thus, clay mineral-bound water is used to uniformly indicate adsorbed water and structural water. As T_1/T_2 increases, asphaltene can be observed with a larger T_1/T_2 value of 100–3000, which is then marked as G. Kerogen (H) has the largest T_1/T_2 value of more than 3000, indicating solid protons (Li et al., 2018b). However, regions F, G, and H may be difficult to distinguish accurately and overlap due to the diversity of organic matter content, maturity, and mineral compositions of shales (Fleury et al., 2013; Li et al., 2020).

However, the T_1–T_2 spectrum of SO shale has been noted to be significantly different, as illustrated in Fig. 6(b). The labels B, C, and D refer to the adsorbed, bound, and movable oils in shale pores, respectively. The T_1/T_2 values are much lower than those in Fig. 6(a), which also differs from the shale sourced from the Shahejie Formation in Dongying Sag, Bohai Bay Basin, in the authors' previous study (Zhang et al., 2020). For the T_1–T_2 spectrum of SO shale, adsorbed oil is located at T_2 less than 1 ms, whereas the T_2 of bound oil ranges from 1 ms to 20 ms. Moreover, movable oil has the largest T_2, more than 20 ms. Based on these two T_1–T_2 patterns, the microscopic occurrence and distribution of oil and water in shale pore systems can be well analyzed.

3.2.3. NMR T_1–T_2 spectra

In this study, shales were analyzed at six different states, namely, at AR, WR-AR, WOR-AR, Dry, SO, and WR, as shown in Fig. 7, respectively. As per the T_1–T_2 patterns presented in Fig. 6, capillary-bound water (A) is obvious, while the adsorbed and free oil peaks are weak in the AR shale T_1–T_2 spectra. Moreover, the (pseudo-)solid protons associated with clay mineral-bound water, asphaltene, and kerogen can also be identified. After water restoration of AR shales, water re-entered the shale pore systems, which led to a dramatic increment of peak A related to capillary-bound water. However, peak E remains difficult to observe, indicating that capillary-bound water mainly consists of shale pore water and thus can escape during coring and sample preparation. It can also be observed that peaks B and C simultaneously changed, which means that the microdistributions of adsorbed and bound oil were affected by water. Moreover, the signal changes of clay mineral-bound water are unpronounced. Thus, the clay mineral-bound water is almost immovable and does not lose.

When the WR-AR shales were saturated with n-dodecane, i.e., WOR-AR state, peak C was noted to increase dramatically, while peak B changed slightly; this could imply that a large amount of bound oil was lost during the coring and sample preparation processes. Compared with AR states, the faint movable oil peaks (D) can be identified, indicating that movable oil was almost lost. The minor changes of peak A are also identified, corresponding to the slightly decreasing of p1 peaks in T_2 spectra at WOR-AR state (Fig. 5). Moreover, T_2 and T_1–T_2 spectra of AR and WOR-AR shales show that parts of capillary-bound water and bound oil, and almost all movable oil were lost for the AR shales. This will be further

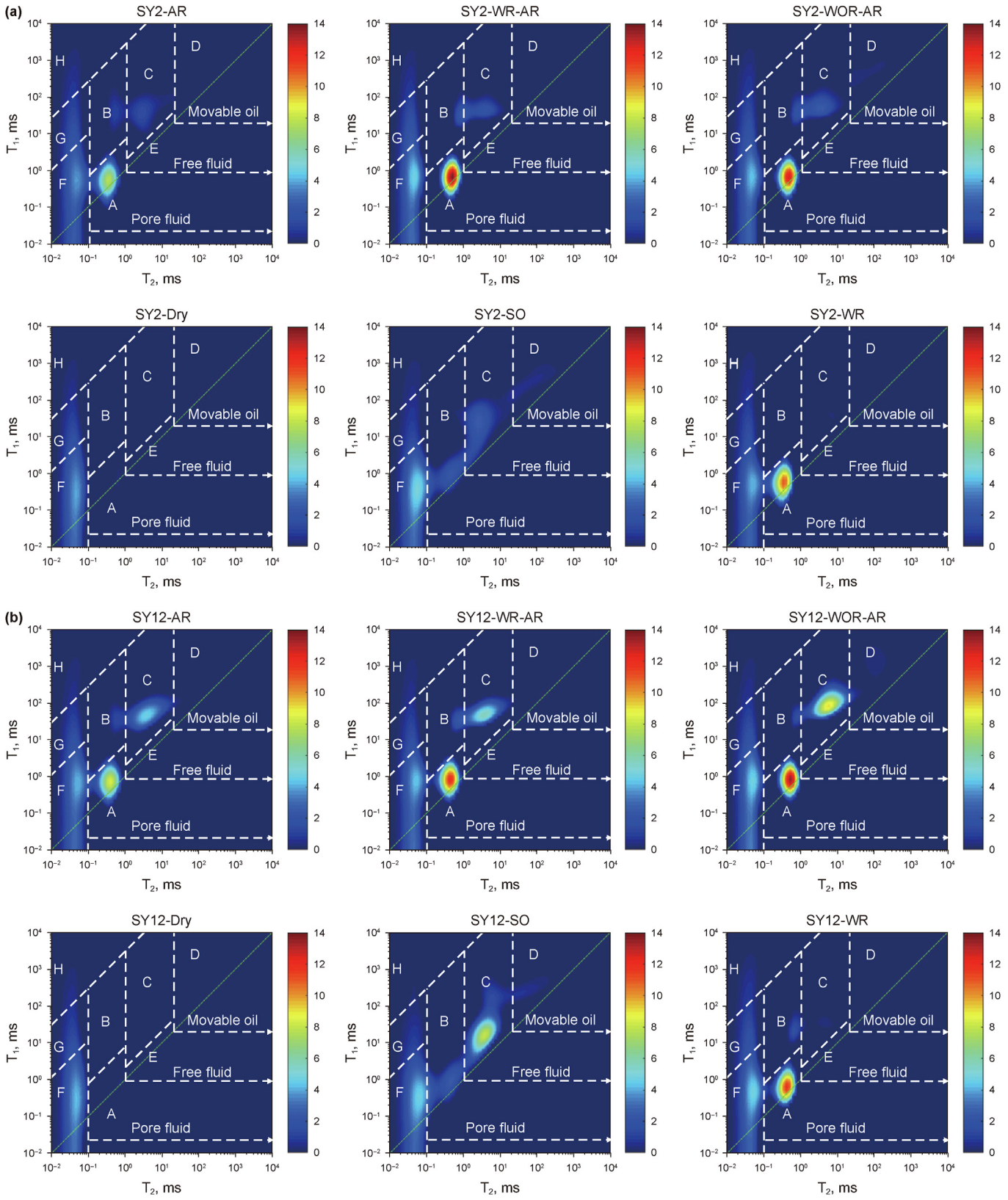

Fig. 7. T_1-T_2 spectra of shales at different states (SY2 and SY12 as examples).

discussed in the next section. After oil-washed and dried, the signals of pore fluids (A–E) completely disappeared, implying that all the pore fluids were extracted. However, the peaks F, G, and H were almost invariable, indicating the (pseudo-)solid protons and poor mobility of clay mineral-bound water, asphaltene, and kerogen. This phenomenon is noted to be consistent with the T_1–T_2 spectra of the post-clean shales in previous studies (Li et al., 2018b; 2020; Zhang et al., 2020). After oil was saturated, the peaks of adsorbed, bound, and movable oils increased expectedly as compared with dry shales. Moreover, WR shales generally had lower signal amplitudes of peaks A than those of WR-AR shales, indicating that water sorption of dry shale may not be an ideal technique to reconstruct in-situ water saturation (Seemann et al., 2017; Chen et al., 2021b).

The discussed NMR T_1–T_2 spectra of shales at six different states (AR, WR-AR, WOR-AR, Dry, SO, and WR) demonstrated the relaxation characteristics and dynamic changes of pore fluids and (pseudo-)solid protons. The (pseudo-)solid protons, i.e., clay mineral-bound water, asphaltene, and kerogen, are almost invariant at different states. However, pore fluids were noted to vary dramatically, especially for capillary-bound water and bound oil, which is consistent with the results indicated from the T_1–T_2 spectra of the fresh shale samples (Li et al., 2020; Liu et al., 2022). Thus, it can be concluded that capillary-bound water and bound oil primarily contribute to the loss of shale pore fluids.

3.3. Changes in water and oil in different states

To further disclose the dynamic changes of pore fluids in shales at different states and verify the accuracy of the T_1-T_2 pattern, the amplitudes of regions A–E in T_1–T_2 spectra were quantitatively extracted and analyzed in this section.

3.3.1. Analyses of oil and water escape in in-situ shales

The T_1–T_2 spectra of sample SY1 at AR and WR-AR states are shown in Fig. 8(a) and (b); this is considered a good example that indicates the loss of capillary-bound water after sampling and preprocessing. The signal amplitudes of capillary-bound water, total oil, adsorbed oil, and bound oil from WR-AR shales are also compared with those from AR shales, as displayed in Fig. 8(c)–(f). The capillary-bound water amplitudes of WR-AR shales are noted to be all larger than those of AR shales, characterized by a linear correlation with a slope of 1.2844 and a high correlation coefficient of 0.8455 (Fig. 8(c)). This further demonstrates that more than one-fifth of pore water was lost during sampling and pretreatment. Moreover, the total oil amplitudes (sum of adsorbed, bound, and movable oils) of WR-AR shales correlate linearly well with those of AR shales, with the slope and correlation coefficient both closing to 1 (Fig. 8(d)). Thus, total pore oil content remains constant during water restoration. However, the microdistributions of bound and adsorbed oil were changed simultaneously, as water re-entered the shale pore system. As shown in Fig. 8(e) and (f), the adsorbed oil amplitudes of WR-AR shales are all larger than those of AR shales, while bound oil is the opposite. The reason may be that when water re-entered shale pores, it would displace bound oil into smaller pores and then transform into adsorbed oil, increasing adsorbed oil.

Compared to AR shale, the signal intensity of region C in relation to bound oil in WOR-AR shale significantly increased, as shown in Fig. 9(a) and (b). A weak signal in region D (movable oi) in WOR-AR shale can also be identified (Fig. 9(b)). To further demonstrate the changes of shale oil in different states, the asphaltene, adsorbed oil, bound oil, and movable oil are discussed respectively. Compared to the AR shales, the WOR-AR shales generally have lower asphaltene amplitudes (Fig. 9(c)), due to part of asphaltene being dissolved during n-dodecane saturation. Moreover, as a result, the dissolved asphaltene adsorbed on the pore surface, leading to an enhancement in region B (adsorbed oil). As shown in Fig. 9(d), WOR-AR samples commonly have larger adsorbed oil amplitudes than AR samples. Bound oil amplitudes at the WOR-AR state are generally larger than those at the AR state (Fig. 9(e)), further confirming that a large amount of bound oil has been lost during the sampling and preparation processes. Moreover, an excellent positive correlation is also discovered with a high correlation coefficient of 0.9619; this implies that the lost content of bound oil is proportional to the total content. That is, the higher the bound oil (free oil) content, the higher the oil loss, which agrees with the light oil (free oil) correction from the Rock-Eval tests of the authors' previous study (Zhang et al., 2022c). In addition, it has been determined that the movable oil amplitudes of WOR-AR shales are much larger than those of AR shales, further indicating that most of the movable oil is lost.

The dissipation process of pore water and oil in shales can be inferred as follows. When shales were taken to the surface, pore water and oil simultaneously escaped outward; this phenomenon could be detected in previous studies (Liu et al., 2022). During this process, most of the movable oil and part of the bound oil were lost, and part of the capillary-bound water (approximately one-fifth in this study) evaporated. Meanwhile, the micro-occurrence and distribution of shale oil also changed. When pore water evaporated, the light oil in adsorbed oil was carried by pore water into large pores and turned into bound oil, while residual heavy components formed asphaltene. Thus, when the water and light oil re-entered into shale pore networks, the signal intensity in region B (adsorbed oil) enhanced, while the signal amplitude in region G (asphaltene) decreased (Fig. 8(e) and 9(c) and 9(d)). The results of the above discussion further demonstrate the accuracy of establishing the T_1-T_2 pattern in this study.

3.3.2. Water distributions of AR and dry shale after water restorations

The equilibrium moisture (water vapor adsorption) method in a controlled RH chamber has been commonly used to reconstruct in-situ pore water distribution in shale (Yang et al., 2020; Cheng et al., 2022). In this study, the equilibrium moisture experiments were conducted on the AR and dry states to obtain WR-AR and WR states. The T_1–T_2 spectra at AR, WR-AR, and WR states are shown in Fig. 10(a)–(c), with sample SY3 as an example; the WR-AR state has the largest signal intensity in region A (capillary-bound water), followed by WR and AR states. The capillary-bound water contents in WR shales are all larger than those in AR shales, while they are generally lower than those of WR-AR shales (Fig. 10(d) and (e)). This finding confirms that equilibrium moisture at high RH (~98%) on dry samples can hardly reconstruct the in-situ pore water distribution in shale (Chen et al., 2021b). The equilibrium moisture experiment has been recommended to be carried out on the AR state to reproduce in-situ pore water distribution.

3.3.3. Effect of pore water on shale oil

Under in-situ conditions, water and oil simultaneously coexist in shale pore networks. The content and microdistribution of pore water directly affect the content and microscopic occurrence of shale oil. To clarify the effect of pore water on shale oil, the T_1–T_2 spectrum at the SO state was compared with the T_1–T_2 spectra at both AR and WOR-AR states, as displayed in Figs. 11 and 12. When pore water exists, the locations of shale oil in the T_1–T_2 spectrum are significantly different from those at SO state, especially for the adsorbed and bound oil (Fig. 11(a), (b), 12(a), 12(b)). In comparison with AR shales, the total oil contents in SO shales correlate linearly well with those in AR shales (Fig. 11(c)); moreover, a better linear correlation (R^2 = 0.9228) is also observed in bound oil contents

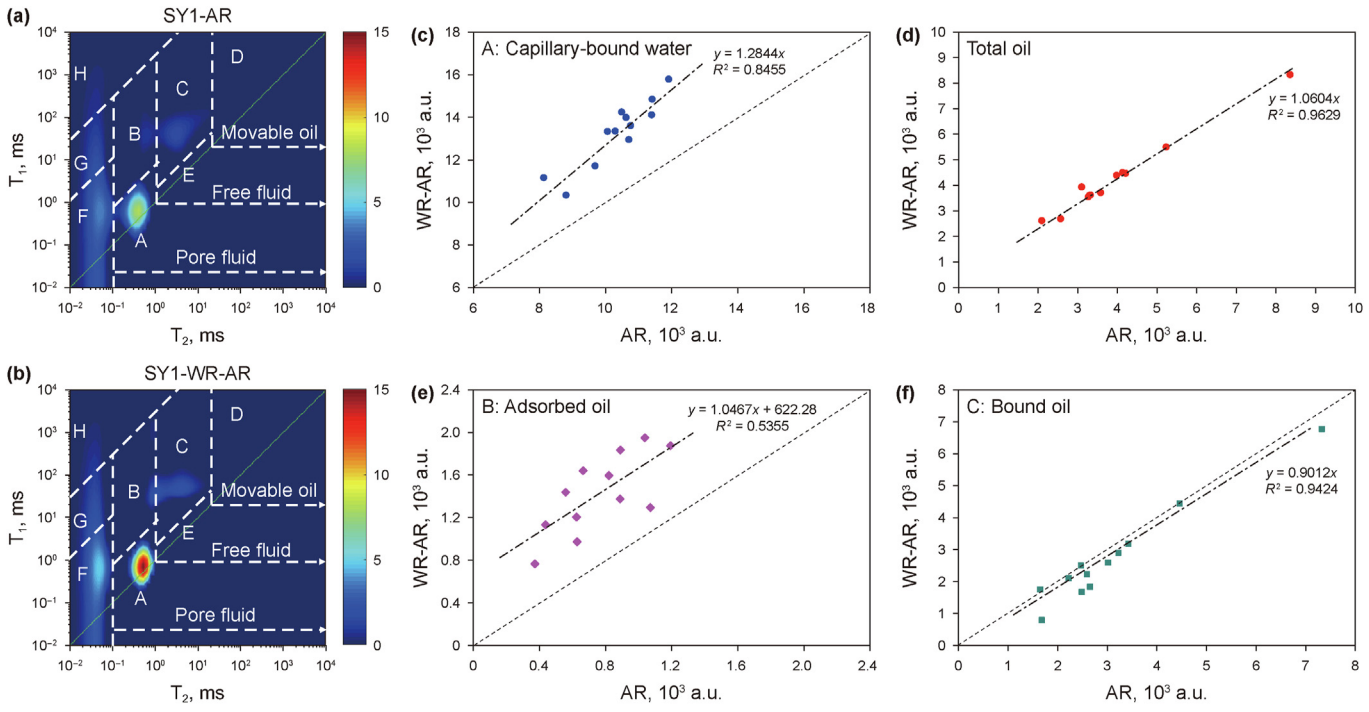

Fig. 8. Comparisons of pore fluids between AR and WR-AR shales.

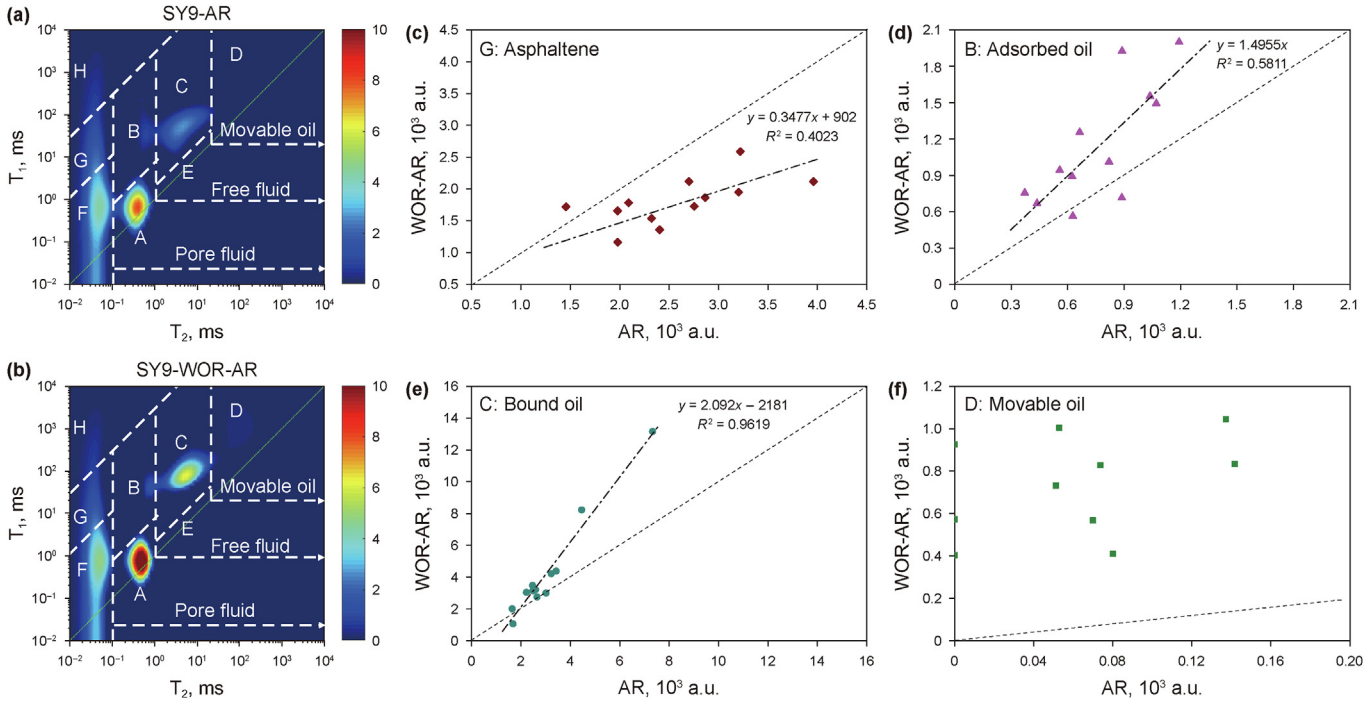

Fig. 9. Comparisons of pore fluids between AR and WOR-AR shales.

between AR and SO shales (Fig. 11(e)). However, a negative correlation of adsorbed oil between AR and SO shales has been identified (Fig. 11(c)). These similar phenomena of total, adsorbed, and bound oils are discovered between WOR-AR and SO shales, as shown in Fig. 12(c)–(e). Thus, it can be found that pore water occupies the storage space and significantly restricts the content and microdistribution of adsorbed oil. Bound oil is also affected by pore water, resulting in a decrease in bound oil. Moreover, bound oil primarily contributes to the total oil content in the shale pore system.

Due to the loss of most movable oil, a negative correlation of movable oil between AR and SO shales was noted (Fig. 11(f)). However, a positive correlation exists between WOR-AR and SO shales, characterized by a slope closing to 1 (Fig. 12(f)); this means that movable oil is almost unaffected by pore water. Thus, it can

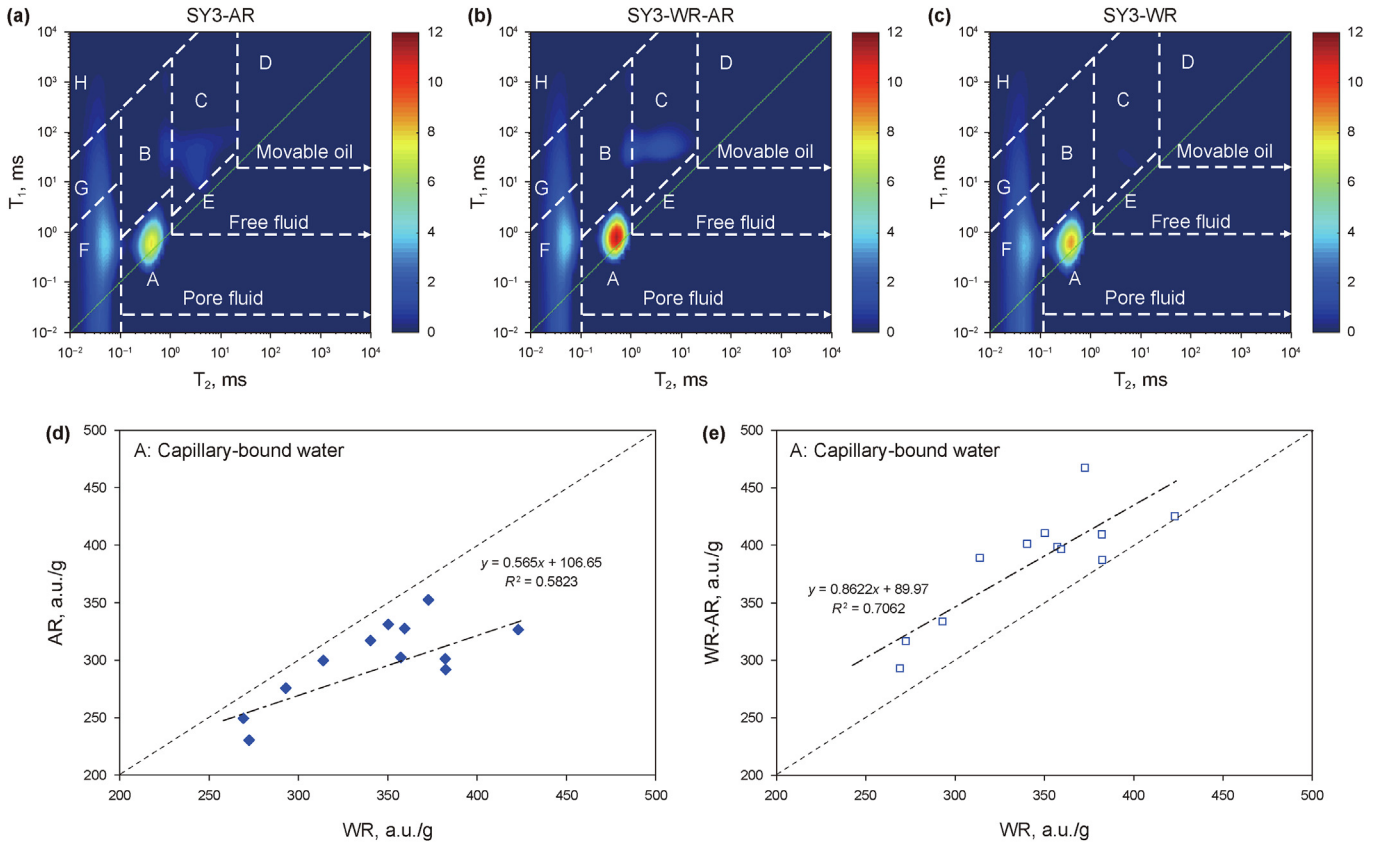

Fig. 10. Water distributions of AR and dry shales after water sorption.

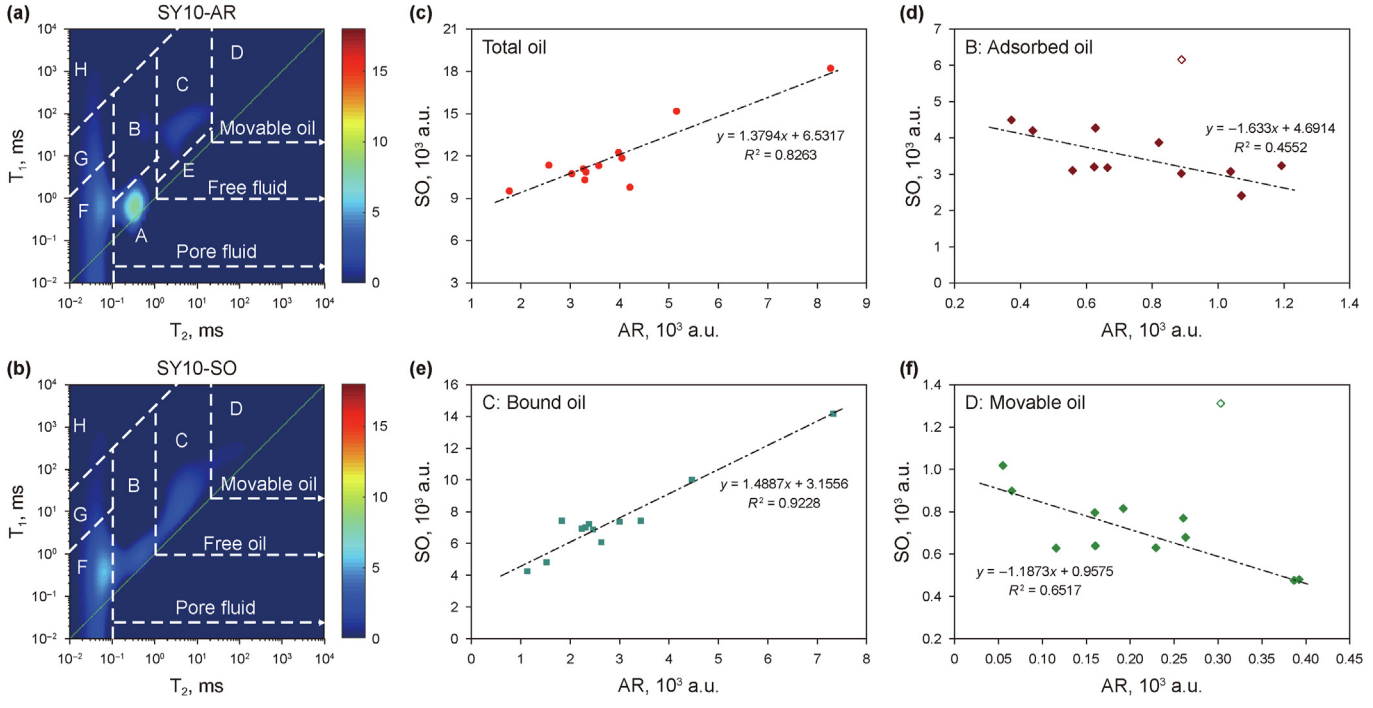

Fig. 11. Comparisons between AR and SO shales.

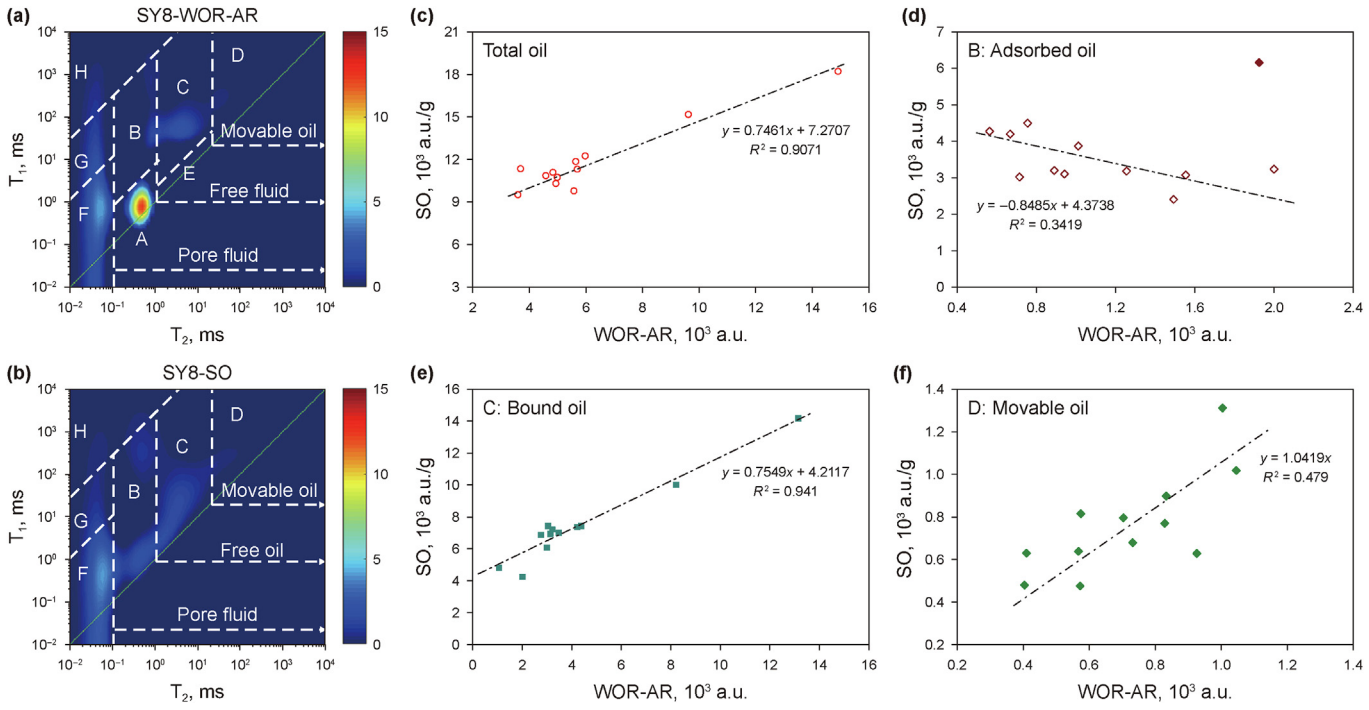

Fig. 12. Comparisons between WOR-AR and SO shales.

conclude that pore water prominently restricts adsorbed oil occurrence, followed by bound oil, but has almost no effect on movable oil.

3.4. Quantitative assessment of water and oil in shales

3.4.1. Calibrations of water and oil in NMR T_1–T_2 spectrum

In order to analyze the pore water and oil contents in shales, the amplitudes of water and oil in the T_1–T_2 spectrum were calibrated. The calibration equation of pore water was determined by comparing the T_1–T_2 spectra at Dry and WR states. An excellent linear correlation exists between the contents and amplitudes of pore water, with a correlation coefficient of 0.9793, as displayed in Fig. 13(a). The pore oil calibration equation was obtained based on the T_1–T_2 spectra at Dry and SO states. An excellent linear correlation has been observed between contents and amplitudes of pore oil (Fig. 13(b)). As per the calibration equations of pore water and oil, the capillary-bound water, movable water, adsorbed oil, bound oil, and movable oil contents can be quantitatively calculated from T_1–T_2 spectra.

The calculation results are listed in Tables 2 and 3 and Fig. 14. The shale pore water at AR state mainly consists of capillary-bound water. The contents of capillary-bound water range from 16.18 mg/g to 24.50 mg/g, with a mean of 20.95 mg/g. For AR shale, shale oil primarily consists of adsorbed and bound oil, but little movable oil. Adsorbed oil varies from 0.90 mg/g to 2.94 mg/g, with an average of 1.87 mg/g, while bound oil is between 3.99 mg/g and 18.69 mg/g (mean 7.64 mg/g). Movable oil contents at AR state are determined to be low, with an average of 0.22 mg/g (0.12–0.35 mg/g). Shale oil (total oil) contents average 9.67 mg/g, ranging from 5.07 mg/g to 21.30 mg/g, with high contents of free oil (bound and movable oils) between 4.13 mg/g and 19.04 mg/g (mean 7.79 mg/g).

After water and oil restoration, pore water and oil contents were noted to increase (Fig. 14). The average capillary-bound water increases to 25.91 mg/g (19.88–31.30 mg/g). The adsorbed oil is between 1.40 mg/g and 4.92 mg/g (mean 2.80 mg/g), while bound oil ranges from 2.61 mg/g and 33.53 mg/g (mean 10.65 mg/g). The movable oil contents increase remarkably, with an average of

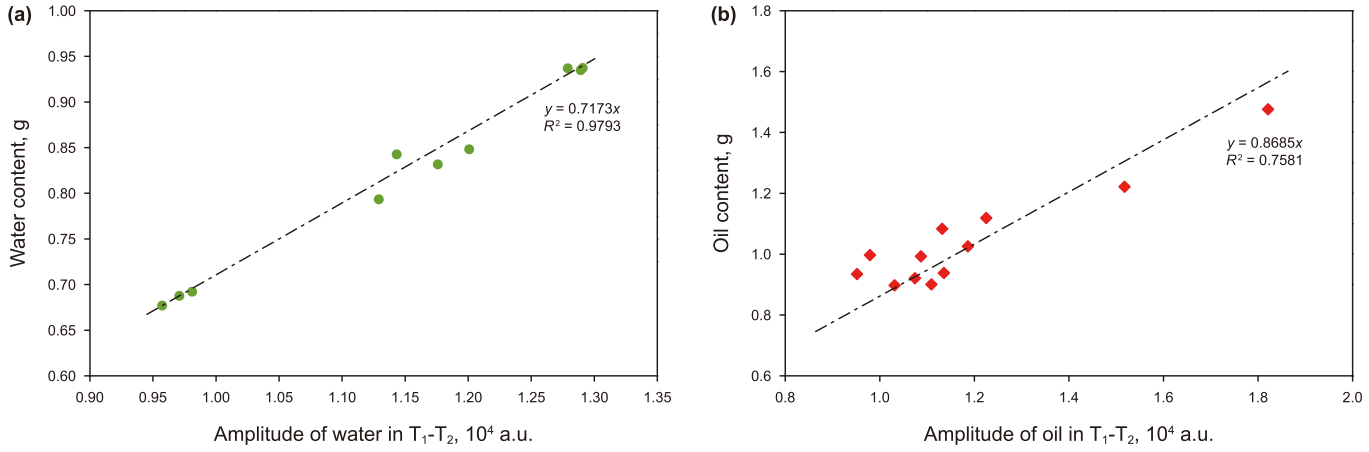

Fig. 13. Calibrations of shale pore water **(a)** and oil **(b)** amplitudes in T_1-T_2 spectra.

Table 2
Shale pore water and oil contents obtained from T_1-T_2 spectra at AR state.

Sample	Capillary-bound water, mg/g	Adsorbed oil, mg/g	Bound oil, mg/g	Movable oil, mg/g	Total oil, mg/g	Free oil, mg/g
SY1	21.10	1.60	6.39	/	7.99	6.39
SY2	21.00	2.52	6.03	0.13	8.67	6.16
SY3	19.32	2.59	5.37	/	7.96	5.37
SY4	23.08	2.01	7.92	0.20	10.13	8.12
SY5	16.18	1.35	5.96	0.17	7.47	6.12
SY6	22.84	0.90	3.99	0.18	5.07	4.17
SY7	17.49	1.50	6.23	0.12	7.86	6.36
SY8	20.93	2.94	7.43	/	10.36	7.43
SY9	22.00	1.55	11.05	0.35	12.95	11.40
SY10	24.50	1.09	8.53	0.29	9.91	8.82
SY11	20.43	2.19	4.13	/	6.32	4.13
SY12	22.54	2.26	18.69	0.35	21.30	19.04

Note: The mark "/" indicates that it has not been detected.

Table 3
Shale pore water and oil contents obtained from T_1-T_2 spectra at WOR-AR state.

Sample	Capillary-bound water, mg/g	Adsorbed oil, mg/g	Bound oil, mg/g	Movable oil, mg/g	Total oil, mg/g	Free oil, mg/g
SY1	26.73	3.02	6.63	1.38	11.03	8.01
SY2	26.92	3.77	7.61	2.43	13.81	10.04
SY3	21.76	3.61	7.35	0.98	11.94	8.33
SY4	26.69	2.48	10.35	1.01	13.84	11.36
SY5	21.94	2.27	8.38	1.37	12.02	9.75
SY6	28.23	1.83	4.88	2.01	8.72	6.89
SY7	19.88	2.14	7.73	1.76	11.63	9.49
SY8	26.37	4.92	7.39	1.41	13.73	8.80
SY9	26.71	1.40	20.37	2.06	23.83	22.43
SY10	31.30	1.66	10.92	2.31	14.88	13.22
SY11	26.77	4.73	2.61	1.73	9.08	4.35
SY12	27.58	1.82	33.53	2.67	38.02	36.20

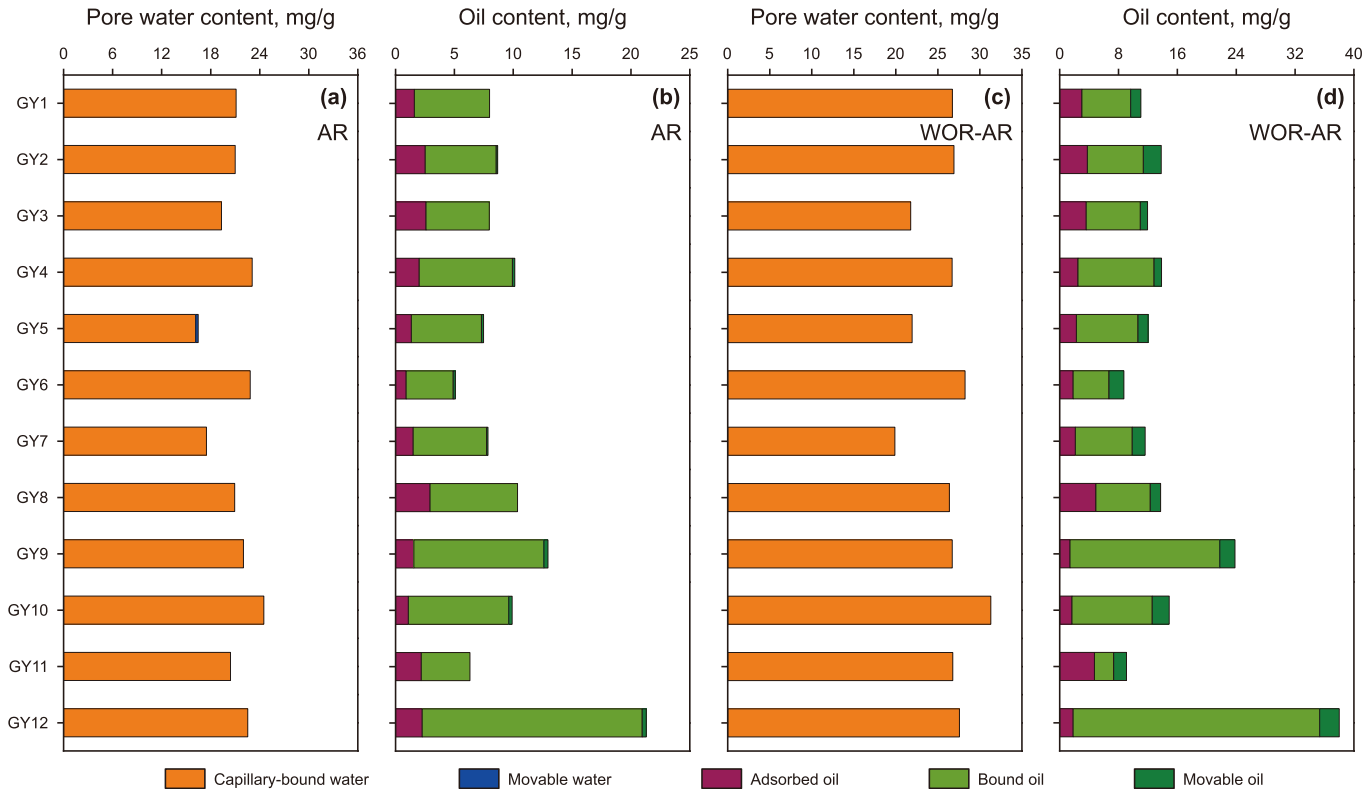

Fig. 14. Shale pore water and oil content distributions in AR ((**a**) and (**b**)) and WR-AR ((**c**) and (**d**)) shales.

1.76 mg/g (0.98–2.67 mg/g). The average total oil increases to 15.21 mg/g, from 8.72 mg/g to 38.02 mg/g. Free oil primarily contributes to pore oil, with a large average content of 12.40 mg/g, varying from 4.35 mg/g to 36.20 mg/g.

3.4.2. Relationships between NMR T_1–T_2 and multistage Rock-Eval

The Rock-Eval technique has been regarded as an accurate quantitative experimental method for analyzing shale oil content. Recently, an improved multistage Rock-Eval technique was established for shale oil content in different occurrence states, such as adsorbed oil ($S_{2\text{-}2}$) and free oil ($S_{1\text{-}1}$+$S_{1\text{-}2}$) (Jiang et al., 2016; Li et al., 2020; Zhang et al., 2022c). In this study, NMR T_1–T_2 spectra were used to calculate the adsorbed, bound, and movable oil contents of AR shales. The total, adsorbed, and free oil of all selected samples from multistage Rock-Eval and T_1–T_2 spectra were compared and analyzed to further determine the shale oil occurrence characteristics, as exhibited in Fig. 15. The total oil contents from T_1–T_2 spectra demonstrate an excellent linear correlation with those from Rock-Eval tests (Fig. 15(a)). The correlation coefficient is equal to 0.9372, demonstrating that NMR T_1–T_2 spectrum can accurately evaluate shale oil content. Moreover, it can also be found that total oil contents from T_1–T_2 spectra are generally larger than those determined using multistage Rock-Eval. A similar phenomenon has been found to occur in free oil contents, as shown in Fig. 15(b). The free oil from the T_1–T_2 spectrum is larger than that from multistage Rock-Eval. The reason may be that multistage Rock-Eval analyses were conducted on powdered shales, thus resulting in more volatile component losses in bound oil, corresponding to lower total and free oil contents.

Surprisingly, the adsorbed oil contents from T_1–T_2 spectra are almost all lower than those measured by multistage Rock-Eval, and a positive correlation is observed, but with a lower correlation coefficient (R^2 = 0.5615), except for three samples, as shown in Fig. 15(c). The reason is speculated as follows. The adsorbed oil obtained from the T_1–T_2 spectrum refers to the oil adsorbed on the pore surface, which is called pore adsorbed oil. However, shale oil cannot only adsorb on the pore surface but also be more soluble with kerogen, and the latter is called absorbed hydrocarbons or oil (Song et al., 2015). In the T_1–T_2 spectrum, absorbed hydrocarbons generally have smaller T_2 but larger T_1/T_2 values, typically occurring in regions G or H, due to weaker flowability. Thus, the adsorbed oil from the T_1–T_2 spectrum is lower than the measured value from the multistage Rock-Eval. This interpretation may be demonstrated by Fig. 15(d). The absorbed hydrocarbons, i.e., the difference between the adsorbed oil from the T_1–T_2 spectrum and the measured value by multistage Rock-Eval, exhibit a weak positive correlation with $S_{2\text{-}2}$, which is related to kerogen. However, the weak positive correlations in Fig. 15(c) and (d) imply that more measurements need to be conducted to further reinforce the correlations.

This demonstrates that the 2D NMR T_1–T_2 is an alternative and accurate technique for analyzing the contents and micro-occurrences of shale oil in different states, and the division method of the T_1–T_2 spectrum in this study is feasible for detecting shale pore water and oil. Moreover, the advantage of NMR over Rock-Eval is that NMR is non-destructive and can be directly conducted on the core samples without being powdered. After water and oil restorations (WOR-AR state), the total oil content in the shale pore network can be well evaluated, which may be deemed

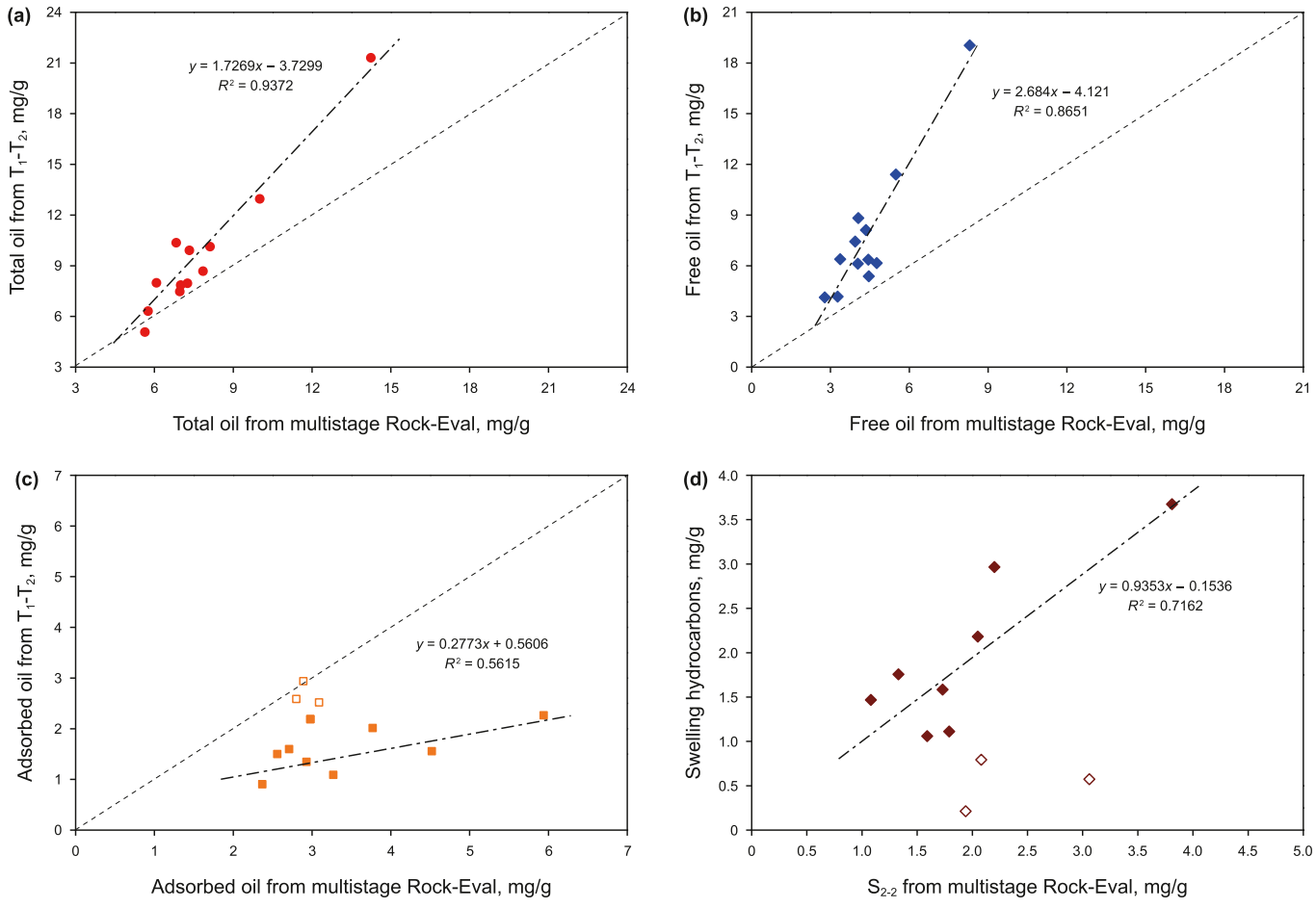

Fig. 15. Relationships between NMR T_1-T_2 and multistage Rock-Eval.

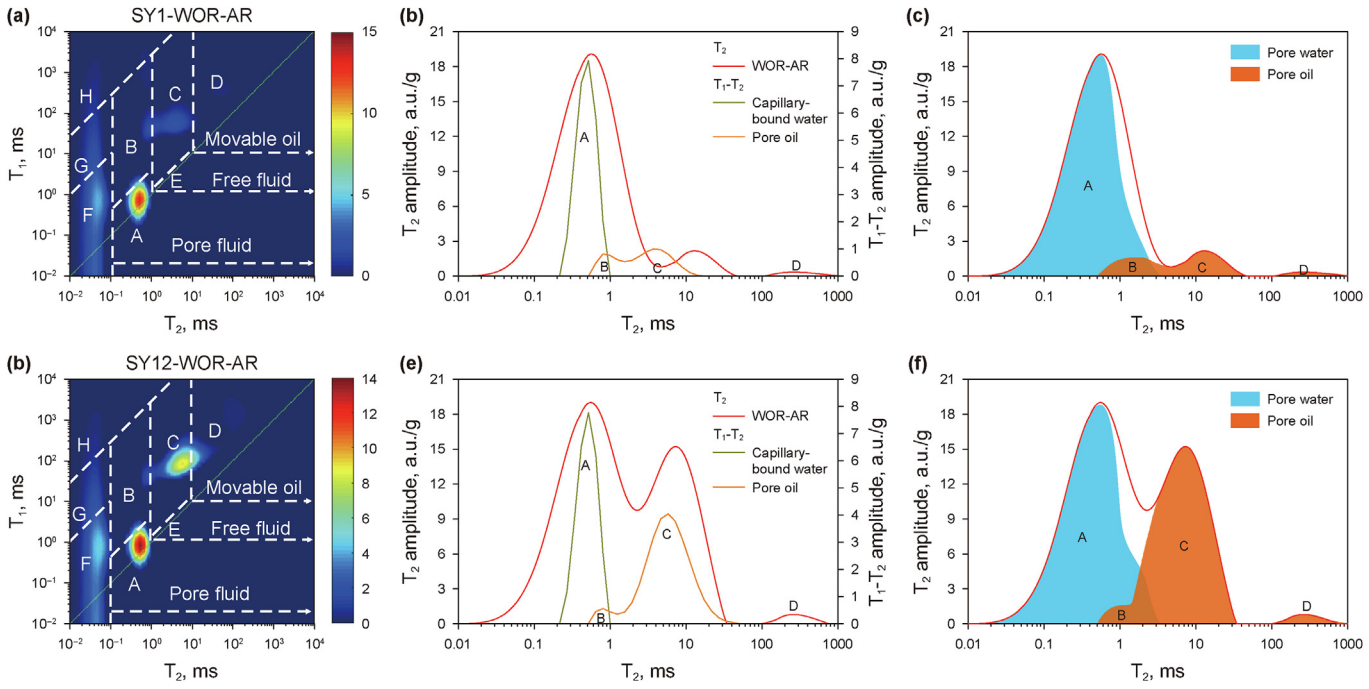

Fig. 16. Microscopic distributions of shale pore water and oil A, B, C, and D refer to the capillary-bound water, adsorbed oil, bound oil, and movable oil, respectively.

more suitable for estimating shale oil reserves. As shale oil production is primarily associated with pore oil, especially free oil, absorbed hydrocarbons in kerogen hardly contribute.

3.5. Microdistributions of shale pore water and oil

As discussed earlier, pore fluids in shales detected via NMR are known to be comprised capillary-bound water as well as shale oil in adsorbed, bound, and movable states. However, the traditional T_2 spectrum has been identified as the comprehensive reflection of all protons in shale, which posed a challenge in terms of directly analyzing the microdistributions of pore oil and water. Thus, in this study, the T_2 and T_1–T_2 spectra at WOR-AR states were used to analyze the microdistributions of shale pore water and oil (Fig. 16).

Pore fluids in shales can be accurately identified in T_1–T_2 spectra, as displayed in Fig. 16(a) and (d). Thus, the T_2 spectra of pore water and oil derived from the T_1–T_2 spectrum can be effectively distinguished. The T_2 spectra of pore water and oil are often characterized by distinct T_2 value intervals (Fig. 16(b) and (e)). The pore water mainly located in T_2 ranges from 0.2 ms to 1 ms, while the T_2 of pore oil is larger than 0.4 ms. Moreover, the pore oil T_2 spectra are bimodal, corresponding to adsorbed and bound oil, respectively.

Nevertheless, inconsistent phenomena were observed between traditional T_2 and T_2 spectra derived from T_1–T_2 spectra. The traditional T_2 spectra are found to be more accurate and have larger T_2 intervals from 0.01 ms to 1000 ms. The T_2 spectra in Fig. 16 have been removed from the signals of the dry samples, corresponding to the signals related to regions F–H in T_1–T_2 spectra. The T_2 spectra in Fig. 16 reflect pore water and oil. In this study, according to the T_1–T_2 and the derived T_2 spectra of pore water and oil, the capillary-bound water, adsorbed oil, bound oil, and movable oil in traditional T_2 spectra can be differentiated, as shown in Fig. 16(c) and (f). The capillary-bound water is primarily located in T_2 less than 3 ms, with a peak at approximately 0.5 ms, followed by adsorbed oil with a peak at approximately 1–2 ms. Bound oil mainly corresponds to the second peak in the traditional T_2 spectrum, ranging from 2 ms to 40 ms, with a peak at approximately 10–20 ms. The tiny right peak is mainly associated with movable oil, which is characterized by the largest T_2 value with a peak at approximately 300 ms. Thus, in the traditional T_2 spectrum, as the T_2 value increases, it sequentially refers to capillary-bound water, adsorbed oil, bound oil, and movable oil. Due to T_2 being proportional to pore size, capillary-bound water, adsorbed oil, bound oil, and movable oil successively occur in micropores to macropores. Capillary-bound water mainly occurs in micropores and can hardly flow because of the immense capillary force. Adsorbed, bound, and movable oils are primarily related to the micropores, mesopores, and macropores, respectively, which is consistent with the authors' previous studies based on oil-saturated shales (Zhao et al., 2022). Both capillary-bound water and adsorbed oil mainly occur in the micropores, resulting in capillary-bound water significantly restricting the micro-occurrence of adsorbed oil, which agrees well with the discussion in Section 3.3.3. The movable water is overlooked in this study due to the extremely low content.

This study demonstrates that NMR can be an alternative technique in characterizing shale pore fluids. The advantage of NMR over Rock-Eval is that both water and oil at different states in shale pore networks can be accurately and quantitatively evaluated without being powdered, which is deemed beneficial for detecting fluids in-situ pore systems.

4. Conclusions

This study examined the microscopic occurrence and distributions of pore fluids in shales using NMR techniques. The contents and microdistributions of water and oil at different states in pore networks were analyzed. The main conclusions are as follows.

An innovative T_1–T_2 pattern for shale oil reservoirs comprising water and oil, primarily divided into pore fluids and (pseudo-)solid protons, has been proposed. Pore fluids include capillary-bound water, movable water, adsorbed oil, bound oil, and movable oil. Pore oil has a larger T_1/T_2 value as compared to pore water, and it is located above pore water in the T_1–T_2 spectrum. Moreover, the (pseudo-)solid protons consist of clay mineral water, asphaltene, and kerogen, often characterized by increasing T_1/T_2 values.

Excellent linear correlations have been noted between total and free oil derived from NMR T_1–T_2 spectra and multistage Rock-Eval. Both total and free oil from NMR T_1–T_2 spectra are generally larger than those from the multistage Rock-Eval, while adsorbed oil is the opposite, suggesting that NMR can accurately and quantitatively evaluate adsorbed, bound, and movable oils in shale pore networks, without absorbed hydrocarbons in kerogen.

Capillary-bound water primarily occurs in the micropores, while adsorbed, bound, and movable oils are mainly associated with the micropores, mesopores, and macropores, respectively. Thus, pore water significantly restricts the microscopic occurrence and distribution of adsorbed oil. Bound oil is also affected by pore water, which can lead to its decreased content, whereas movable oil is hardly affected.

CRediT authorship contribution statement

Peng-Fei Zhang: Writing – original draft, Methodology, Investigation, Funding acquisition. **Shuang-Fang Lu:** Writing – review & editing, Conceptualization. **Jun-Jie Wang:** Writing – review & editing, Project administration, Formal analysis. **Wen-Biao Li:** Methodology, Funding acquisition. **Ya-Jie Yin:** Methodology, Investigation, Data curation. **Guo-Hui Chen:** Writing – review & editing, Funding acquisition. **Neng-Wu Zhou:** Funding acquisition, Conceptualization. **Han Wu:** Writing – review & editing.

Declaration of competing interest

The authors declare that they have no known competing financial interests or personal relationships that could have appeared to influence the work reported in this paper.

Acknowledgments

This study was financially supported by the National Natural Science Foundation of China (42302160, 42302170, 42302183, and 42072174), the Sanya City Science and Technology Innovation Project (2022KJCX51), and the Support Plan for Outstanding Youth Innovation Team in Shandong Higher Education Institutions (2022KJ060).

Acronyms

NMR	Nuclear magnetic resonance
LTNA/D	Low-temperature nitrogen adsorption and desorption
MICP	Mercury intrusion capillary pressure
1D	One-dimensional
2D	Two-dimensional
RH	Relative humidity
CPMG	Carr-Purcell-Meiboom-Gill
SR-CPMG	Saturation-recovery-Carr-Purcell-Meiboom-Gill
TW	Waiting time
TE	Echo time
NRCH	Echo number
NS	Number of scan
R_o	Vitrinite reflectivity
TOC	Total organic carbon
AR	As-received
WR-AR	Water restoration of as-received
WOR-AR	Water and restoration of as-received
Dry	Oil-washed and dry
SO	Oil-saturated
WR	Water restoration of dry

References

Bai, L., Liu, B., Du, J., Wang, B., Tian, S., Wang, L., Xue, Z., 2022. Distribution characteristics and oil mobility thresholds in lacustrine shale reservoir: Insights from N_2 adsorption experiments on samples prior to and following hydrocarbon extraction. Petrol. Sci. 19, 486–497. https://doi.org/10.1016/j.petsci.2021.10.018.

Birdwell, J., Washburn, K., 2015. Multivariate analysis relating oil shale geochemical properties to NMR relaxometry. Energy Fuel. 29, 2234–2243. https://doi.org/10.1021/ef502828k.

Chen, J., Xu, Y., Cai, H., Xiao, Q., Wen, J., Zhou, Q., Li, T., 2021a. Understanding water accessibility and pore information of overmature marine shales using water vapor sorption. Mar. Petrol. Geol. 130, 105120. https://doi.org/10.1016/j.marpetgeo.2021.105120.

Chen, J., Gai, H., Xiao, Q., 2021b. Effects of composition and temperature on water sorption in overmature Wufeng–Longmaxi shales. Int. J. Coal Geol. 234, 103673. https://doi.org/10.1016/j.coal.2020.103673.

Cheng, P., Xiao, X., Tian, H., Wang, X., 2018. Water content and equilibrium saturation and their influencing factors of the lower paleozoic overmature organic–rich shales in the upper yangtze region of southern China. Energy Fuel. 32, 11452–11466. https://doi.org/10.1021/acs.energyfuels.8b03011.

Cheng, P., Xiao, X., Tian, H., Cai, H., Zhou, Q., Li, T., Fan, Q., 2022. Differences in the distribution and occurrence phases of pore water in various nanopores of marine–terrestrial transitional shales in the Yangquan area of the northeast Qinshui Basin. China. Mar. Petrol. Geol. 137, 105510. https://doi.org/10.1016/j.marpetgeo.2021.105510.

D'Agostino, C., Mitchell, J., Mantle, M., Gladden, L., 2014. Interpretation of NMR relaxation as a tool for characterising the adsorption strength of liquids inside porous materials. Chem. Eur J. 20, 13009–13015. https://doi.org/10.1002/chem.201403139.

Fan, Z., Cheng, P., Tian, H., Cai, H., Xiao, X., 2023. Distribution and occurrence of pore water and retained oil in nanopores of marine–terrestrial transitional shales during oil generation and expulsion: implications from a thermal simulation experiment on shale plug samples. Mar. Petrol. Geol. 150, 106125. https://doi.org/10.1016/j.marpetgeo.2023.106125.

Feng, D., Li, X., Wang, X., Li, J., Sun, F., Sun, Z., Zhang, T., Li, P., Chen, Y., Zhang, X., 2018. Water adsorption and its impact on the pore structure characteristics of shale clay. Appl. Clay Sci. 155, 126–138. https://doi.org/10.1016/j.clay.2018.01.017.

Fleury, M., Kohler, E., Norrant, F., Gautier, S., M Hamdi, J., Barré, L., 2013. Characterization and quantification of water in smectites with low–field NMR. J. Phys. Chem. C 117, 4451–4560. https://doi.org/10.1021/jp311006q.

Fleury, M., Romero-Sarmiento, M., 2016. Characterization of shales using T_1–T_2 NMR maps. J. Petrol. Sci. Eng. 137, 55–62. https://doi.org/10.1016/j.petrol.2015.11.006.

Habina, I., Radzik, N., Topór, T., Krzyżak, A., 2017. Insight into oil and gas–shales compounds signatures in low field 1H NMR and its application in porosity evaluation. Microporous Mesoporous Mater. 252, 37–49. https://doi.org/10.1016/j.micromeso.2017.05.054.

He, W., Liu, B., Zhang, J., Bai, L., Tian, S., Chi, Y., 2023. Geological characteristics and key scientific and technological problems of Gulong shale oil in Songliao Basin. Earth Sci. 48, 49–62. https://doi.org/10.3799/dqkx.2022.320.

Hu, T., Pang, X., Jiang, F., Wang, Q., Liu, X., Wang, Z., Jiang, S., Wu, G., Li, G., Xu, T., Li, M., Yu, J., Zhang, C., 2021. Movable oil content evaluation of lacustrine organic–rich shales: methods and a novel quantitative evaluation model. Earth Sci. Rev. 214, 103545. https://doi.org/10.1016/j.earscirev.2021.103545.

Huangfu, Y., Zhang, J., Zhang, S., He, K., Zhang, B., Tian, H., 2023. Characteristics of shale oil in different occurrence states of Cretaceous Qingshankou Formation in the northern Songliao basin. Acta Geol. Sin. 97, 523–538. https://doi.org/10.3969/j.issn.0001-5717.2023.02.015.

Jia, Z., Xiao, L., Chen, Z., Liao, G., Zhang, Y., Wang, Z., Can, L., Guo, L., 2018. Determining shale organic porosity and total organic carbon by combining spin echo, solid echo and magic echo. Microporous Mesoporous Mater. 269, 12–16. https://doi.org/10.1016/j.micromeso.2017.11.049.

Jiang, Q., Li, M., Qian, M., Li, Z., Li, Z., Huang, Z., Zhang, C., Ma, Y., 2016. Quantitative characterization of shale oil in different occurrence states and its application. Petrol. Geol. Exper. 38, 842–849. https://doi.org/10.11781/sysydz201606842.

Jin, Z., Liang, X., Bai, Z., 2022. Exploration breakthrough and its significance of Gulong lacustrine shale oil in the Songliao Basin, Northeastern China. Energy Geosci. 3, 120–125. https://doi.org/10.1016/j.engeos.2022.01.005.

Li, J., Yin, J., Zhang, Y., Lu, S., Wang, W., Li, J., Chen, F., Meng, Y., 2015. A comparison of experimental methods for describing shale pore features—a case study in the Bohai Bay Basin of eastern China. Int. J. Coal Geol. 152, 39–49. https://doi.org/10.1016/j.coal.2015.10.009.

Li, J., Zou, Y., Xu, X., Sun, J., Li, M., Peng, P., 2016. Adsorption of mudstone source rock for shale oil—experiments, model and a case study. Org. Geochem. 92, 55–62. https://doi.org/10.1016/j.orggeochem.2015.12.009.

Li, J., Li, X., Wu, K., Feng, D., Zhang, T., Zhang, Y., 2017a. Thickness and stability of water film confined inside nanoslits and nanocapillaries of shale and clay. Int. J. Coal Geol. 179, 253–268. https://doi.org/10.1016/j.coal.2017.06.008.

Li, J., Lu, S., Xie, L., Zhang, J., Xue, H., Zhang, P., Tian, S., 2017b. Modeling of hydrocarbon adsorption on continental oil shale: a case study on n–alkane. Fuel 206, 603–613. https://doi.org/10.1016/j.fuel.2017.06.017.

Li, J., Lu, S., Cai, J., Zhang, P., Xue, H., Zhao, X., 2018. Adsorbed and free oil in

lacustrine nanoporous shale: a theoretical model and a case study. Energy Fuel. 32, 12247–12258. https://doi.org/10.1021/acs.energyfuels.8b02953.
Li, J., Wang, S., Lu, S., Zhang, P., Cai, J., Zhao, J., Li, W., 2019. Microdistribution and mobility of water in gas shale: a theoretical and experimental study. Petrol. Geol. 102, 496–507. https://doi.org/10.1016/j.marpetgeo.2019.01.012.
Li, J., Wang, Y., Song, Z., Wang, M., Zhao, J., 2024. Mobility of connate pore water in gas shales: a quantitative evaluation on the Longmaxi shales in the southern Sichuan basin. China. Mar. Petrol. Geol. 161, 106674. https://doi.org/10.1016/j.marpetgeo.2023.106674.
Li, J., Jiang, C., Wang, M., Lu, S., Chen, Z., Chen, G., Li, J., Li, Z., Lu, S., 2020. Adsorbed and free hydrocarbons in unconventional shale reservoir: a new insight from NMR T_1–T_2 maps. Mar. Petrol. Geol. 116, 104331. https://doi.org/10.1016/j.marpetgeo.2020.104311.
Li, J., Jiang, C., Wang, M., Xu, L., Li, M., Yu, C., Wu, Y., Lu, S., 2022. Determination of in situ hydrocarbon contents in shale oil plays. Part 1: is routine Rock–Eval analysis reliable for quantifying the hydrocarbon contents of preserved shale cores? Org. Geochem. 170, 104449. https://doi.org/10.1016/j.orggeochem.2022.104449.
Lin, Z., Li, J., Lu, S., Hu, Q., Zhang, P., Wang, J., Zhi, Q., Huang, H., Yin, N., Wang, Y., Ge, T., 2024. The occurrence characteristics of oil in shales matrix from organic geochemical screening data and pore structure properties: an experimental study. Petrol. Sci. 21, 1–13. https://doi.org/10.1016/j.petsci.2023.09.002.
Liu, B., Bai, L., Chi, Y., Jia, R., Fu, X., Yang, L., 2019. Geochemical characterization and quantitative evaluation of shale oil reservoir by two–dimensional nuclear magnetic resonance and quantitative grain fluorescence on extract: a case study from the Qingshankou Formation in Southern Songliao Basin, northeast China. Mar. Petrol. Geol. 109, 561–573. https://doi.org/10.1016/j.marpetgeo.2019.06.046.
Liu, B., Jiang, X., Bai, L., Lu, R., 2022. Investigation of oil and water migrations in lacustrine oil shales using 20 MHz 2D NMR relaxometry techniques. Petrol. Sci. 19, 1007–1018. https://doi.org/10.1016/j.petsci.2021.10.011.
Liu, X., Lai, J., Fan, X., Shu, H., Wang, G., Ma, X., Liu, M., Guan, M., Luo, Y., 2020. Insights in the pore structure, fluid mobility and oiliness in oil shales of Paleogene Funing Formation in Subei Basin. China. Mar. Petrol. Geol. 114, 104228. https://doi.org/10.1016/j.marpetgeo.2020.104228.
Liu, X., Jin, Z., Lai, J., Fan, X., Guan, M., Shu, H., Wang, G., Liu, M., Luo, Y., 2021. Fractal behaviors of NMR saturated and centrifugal T_2 spectra in oil shale reservoirs: the Paleogene Funing formation in Subei basin. China. Mar. Petrol. Geol. 129, 105069. https://doi.org/10.1016/j.marpetgeo.2021.105069.
Lu, S., Huang, W., Chen, F., Li, J., Wang, M., Xue, H., Wang, W., Cai, X., 2012. Classification and evaluation criteria of shale oil and gas resources: discussion and application. Petrol. Explor. Dev. 39, 249–256. CNKI:SUN:SKYK.0.2012-02-018.
Sang, Q., Zhao, X., Liu, Y., Li, Z., Dong, M., 2022. Effects of the laminated–structure and mixed wettability on the oil/water relative permeabilities and oil productions in shale oil formations. J. Petrol. Sci. Eng. 208, 109457. https://doi.org/10.1016/j.petrol.2021.109457.
Song, L., Xue, H., Lu, S., Tian, S., 2015. Research progress on the occurrence mechanism of detained hydrocarbon. Acta Geol. Sin–Engl. 87, 164–165. https://doi.org/10.1111/1755-6724.12303_6.
Seemann, T., Bertier, P., Krooss, B.M., Stanjek, H., 2017. Water vapour sorption on mudrocks. Geol. Soc. Lond., Spec. Publ. 454, 201–233. https://doi.org/10.1144/SP454.8.
Tian, S., Erastova, V., Lu, S., Greenwell, H., Underwood, T., Xue, H., Zeng, F., Chen, G., Wu, C., Zhao, R., 2018. Understanding model crude oil component interactions on kaolinite silicate and aluminol surfaces: toward improved understanding of shale oil recovery. Energy Fuel. 32, 1155–1165. https://doi.org/10.1021/acs.energyfuels.7b02763.
Wang, M., Ma, R., Li, J., Lu, S., Li, C., Guo, Z., Li, Z., 2019. Occurrence mechanism of lacustrine shale oil in the paleogene Shahejie Formation of jiyang depression, Bohai Bay Basin, China. Petrol. Geol. Exper. 46, 789–802. https://doi.org/10.11698/PED.2019.04.19.
Wang, M., Li, M., Li, J., Xu, L., Zhang, J., 2022a. The key parameter of shale oil resource evaluation: oil content. Petrol. Sci. 19, 1443–1459. https://doi.org/10.1016/j.petsci.2022.03.006.
Wang, X., Wang, M., Li, J., Shao, H., Deng, Z., Wu, Y., 2022b. Thermal maturity: the controlling factor of wettability, pore structure, and oil content in the lacustrine Qingshankou shale, Songliao Basin. J. Petrol. Sci. Eng. 215, 110618. https://doi.org/10.1016/j.petrol.2022.110618.
Xu, Y., Lun, Z., Pan, Z., Wang, H., Zhou, X., Zhao, C., Zhang, D., 2022. Occurrence space and state of shale oil: a review. J. Petrol. Sci. Eng. 211, 110183. https://doi.org/10.1016/j.petrol.2022.110183.
Xue, H., Tian, S., Wang, W., Zhang, W., Du, T., Mu, G., 2016. Correction of oil content–one key parameter in shale oil resource assessment. Oil Gas Geol. 37, 15–22. https://doi.org/10.11743/ogg20160103.
Yang, R., Jia, A., He, S., Hu, Q., Dong, T., Hou, Y., Yan, J., 2020. Water adsorption characteristics of organic–rich Wufeng and Longmaxi shales, Sichuan Basin (China). J. Petrol. Sci. Eng. 193, 107387. https://doi.org/10.1016/j.petrol.2020.107387.
Zhang, J., Zhu, R., Wu, S., Jiang, X., Liu, C., Cai, Y., Zhang, S., Zhang, T., 2023a. Microscopic oil occurrence in high-maturity lacustrine shales: Qingshankou Formation, Gulong sag, Songliao Basin. Petrol. Sci. 20, 2726–2746. https://doi.org/10.1016/j.petsci.2023.08.026.
Zhang, P., Lu, S., Li, J., Chen, C., Xue, H., Zhang, J., 2018. Petrophysical characterization of oil–bearing shales by low–field nuclear magnetic resonance (NMR). Mar. Petrol. Geol. 89, 775–785. https://doi.org/10.1016/j.marpetgeo.2017.11.015.
Zhang, P., Lu, S., Li, J., 2019. Characterization of pore size distributions of shale oil reservoirs: a case study from Dongying sag, Bohai Bay basin. China. Mar. Petrol. Geol. 100, 297–308. https://doi.org/10.1016/j.marpetgeo.2018.11.024.
Zhang, P., Lu, S., Li, J., Chang, X., 2020. 1D and 2D Nuclear magnetic resonance (NMR) relaxation behaviors of protons in clay, kerogen and oil–bearing shale rocks. Mar. Petrol. Geol. 150, 106156. https://doi.org/10.1016/j.marpetgeo.2019.104210.
Zhang, P., Lu, S., Li, J., Chang, X., Lin, Z., Chen, G., Li, J., Liu, J., Tian, S., 2022a. Evaluating microdistribution of adsorbed and free oil in a lacustrine shale using nuclear magnetic resonance: a theoretical and experimental study. J. Petrol. Sci. Eng. 212, 110208. https://doi.org/10.1155/2022/3539482.
Zhang, P., Lu, S., Lin, Z., Duan, H., Chang, X., Qiu, Y., Fu, Q., Zhi, Q., Wang, J., Huang, H., 2022c. Key oil content parameter correction of shale oil resources: a case study of the paleogene funing formation, subei basin, China. Energy Fuel. 36, 5316–5326. https://doi.org/10.1021/acs.energyfuels.2c00610.
Zhang, P., Yin, Y., Lu, S., Li, J., Chang, X., Zhang, J., Pang, Y., Chen, G., Liu, Y., Li, Z., 2022d. Insights into pore structures and multifractal characteristics of shale oil reservoirs: a case study from dongying sag, Bohai Bay Basin, China. Energy Fuel. 36, 8224–8237. https://doi.org/10.1016/j.marpetgeo.2017.11.015.
Zhang, P., Lu, S., Li, J., Chang, X., Zhang, J., Pang, Y., Lin, Z., Chen, G., Yin, Y., Liu, Y., 2023b. Quantitative characterization of shale pore connectivity and controlling factors using spontaneous imbibition combined with nuclear magnetic resonance T_2 and T_1-T_2. Petrol. Sci. 20, 1947–1960. https://doi.org/10.1016/j.petsci.2023.03.011.
Zhang, W., Feng, Q., Wang, S., Zhang, J., Jin, Z., Xie, T., Xing, X., Lv, P., 2022b. Pore network modeling of oil and water transport in nanoporous shale with mixed wettability. J. Petrol. Sci. Eng. 209, 109884. https://doi.org/10.1016/j.petrol.2021.109884.
Zhao, W., Hu, S., Hou, L., Yang, T., Lin, X., Guo, B., Yang, Z., 2020. Types and resource potential of continental shale oil in China and its boundary with tight oil. Petrol. Explor. Dev. 47, 1–10. https://doi.org/10.11698/PED.2020.01.01.
Zhao, P., He, B., Zhang, B., Liu, J., 2022. Porosity of gas shale: is the NMR-based measurement reliable? Petrol. Sci. 19, 509–517.
Zolfaghari, A., Dehghanpour, H., Holyk, J., 2017. Water sorption behaviour of gas shales: I. Role of clays. Int. J. Coal Geol. 179, 130–138. https://doi.org/10.1016/j.coal.2017.05.008.